

OBSERVATIONS OF ENERGY AND WATER VAPOR FLUXES ON A LIVING ROOF
SURFACE

A Thesis submitted to the faculty of
San Francisco State University
In partial fulfillment of
the requirements for
the Degree

Master of Arts

In

Geography

by

Siobhan Casey Lavender

San Francisco, California

January 2015

CERTIFICATION OF APPROVAL

I certify that I have read Impacts of living roofs on urban climate in San Francisco California by Siobhan Casey Lavender, and that in my opinion this work meets the criteria for approving a thesis submitted in partial fulfillment of the requirement for the degree Master of Art in Geography at San Francisco State University.

Andrew Oliphant, Ph.D.
Professor of Geography

Leonhard Blesius, Ph.D.
Associate Professor of Geography

OBSERVATIONS OF ENERGY AND WATER VAPOR FLUXES ON A LIVING ROOF SURFACE

Siobhan Casey Lavender
San Francisco, California
2015

The results from this study offer a micrometeorological profile of an extensive/intensive living roof in the Mediterranean climate of San Francisco California, specifically the roof's impact on the surface radiation budget and surface energy balance. Living roofs have long been touted for their ability to positively impact microclimate by reflecting solar radiation and cooling the atmosphere through the latent heat flux, thereby offsetting adverse effects of the urban heat island effect (UHI). This is the first study using the eddy covariance technique on a living roof, and was achievable due to the roof's large (one hectare) size and stringent (~50%) data rejection. The annual average albedo of the living roof was 0.20 with a seasonal monthly maximum of .22 and a minimum of 17.39. The annual ensemble average partitioning of energy balance terms indicated that latent and sensible heat fluxes were close to equal with an annual Bowen ratio of 0.96. On a diurnal temporal scale, the sensible heat began to surpass the latent heat in the mid-morning, and on a seasonal timescale, sensible heat dominated the energy balance partitioning in the late summer and early spring, and was overtaken by the latent heat flux in the fall and winter. The latent heat flux produced an annual average cooling rate of 3.19 ($\text{MJ m}^{-2} \text{ dy}^{-1}$). Ground heat flux observations indicated that the substrate acted as insulation, with a small average diurnal maximum of 3 (W m^{-2}) of heat energy entering the building below. Energy balance closure as determined by linear regression showed that the turbulent fluxes underestimated available energy by 38% ($R^2 = 0.92$).

I certify that the Abstract is a correct representation of the content of this thesis.

Chair, Thesis Committee

Date

PREFACE AND/OR ACKNOWLEDGEMENT

This work is due wholly to the tireless dedication and oversight of Professor Andrew Oliphant who has been the driving force behind my interest and love of this subject matter. My sincere gratitude to him for guiding me through this project and the supporting microclimatological theory to which I had not been previously exposed. Also many thanks to Professor Leonard Blesius who agreed to second this thesis project despite sitting on numerous other committees this semester; his keen editing skills and knowledge of physical geography have been a major asset. Thank you to Ryan Thorp for spearheading the original 2013 deployment of the micrometeorological tower and for his astute analysis of that deployment's data, as well as his and Suzanne Maher's aid in installing the equipment again in 2014. Thanks to Craig Clements and San Jose State University for equipment calibration assistance. Lastly without the support of the California Academy of Sciences and our point-of-contact Kendra Hauser, who gave us continuous access to the roof and provided ecological and maintenance expertise, this project would not have been possible.

TABLE OF CONTENTS

List of Tables	vii
List of Figures.....	viii
1.0 Background and Introduction.....	1
1.1 Urban climates and vegetation cover	1
1.2 UHI and PCI.....	1
1.3 Living roofs	3
1.4. The surface energy balance and radiation budget.....	6
2.0 Study Site	8
2.1. Location and background.....	8
2.2. Subsurface roof structure.....	11
2.3. Ecology and vegetation surveys.....	12
3.0 Materials and Methods	15
3.1. Deployment.....	15
3.2. Project footprint.....	17
3.3. Determining the ground heat flux	19
4.0 Results	21
4.1. Surface radiation budget	22
4.2. Surface energy balance	27
4.3. Controls on the surface energy balance	31
4.4. Ground heat flux	34
4.5. Annual comparison	37

4.6. Energy balance closure.....	41
5.0 Discussion.....	43
5.1. Surface albedo.....	43
5.2. Living roof controls on surface energy balance	45
5.3. Ground heat conduction and storage	48
5.4. Controls on energy balance closure and sources of error.....	49
6.0 For future study: Comparing latent heat flux	51
7.0 Conclusions.....	52
8.0 References.....	56

LIST OF TABLES

Table	Page
1. Classifications of living roofs (Berardi et al. 2014).....	10
2. List of plant species and percent cover of each on the living roof of the California Academy of Sciences in San Francisco Ca, 2014.....	14
3. Biomicrometeorological instruments deployed on the California Academy of Sciences' living roof, San Francisco Ca, 2013-2015.....	16
4. Total study period and monthly totals (in MJ m ⁻² dy ⁻¹) for the component parts of the surface radiation budget. Measured on the living roof of the California Academy of Sciences, San Francisco, Ca, 2014-15.....	24
5. General monthly meteorological conditions between April 2014 and March 2015 on the California Academy of Sciences' living roof, San Francisco, Ca.....	28
6. Total study period and monthly total values of energy balance terms as well as the Bowen ratio and residual (in MJ m ⁻² dy ⁻¹). Measured on the living roof of the California Academy of sciences, San Francisco, Ca.....	30
7. Monthly values of ground heat flux terms (in MJ m ⁻² dy ⁻¹). Measured on the living roof of the California Academy of Sciences, San Francisco, Ca. October 2014 – February 2015.....	37
8. Monthly total shortwave radiation for 2013 and 2014 (n MJ m ⁻² dy ⁻¹) Measured on the living roof of the California Academy of sciences, San Francisco, Ca.....	38
9. Monthly totals for 2013 and 2014 (in MJ m ⁻² dy ⁻¹) for the component parts of the surface energy balance. Measured on the living roof of the California Academy of Sciences, San Francisco, Ca.....	38

LIST OF FIGURES

Figures	Page
1. Location of the study tower (a) on the west coast of the US in the state of California (b), within the eastern span of the Golden Gate park in San Francisco and (c) on the southeast corner of the California Academy of Sciences' Living roof (Google Earth).....	9
2. Visual evidence of seasonal variation in vegetation vitality on the California Academy of Sciences' living roof, in San Francisco Ca for the months of (a) May 2014, (b) August 2014 and (c) February 2015.....	9
3. Schematic of the living roof structure on the California Academy of Sciences, San Francisco, Ca.....	12
4. Researchers conducting point sampling for vegetation surveys on the living roof of the California Academy of Sciences, San Francisco Ca, 2014.....	14
5. April 2014 – March 2015 diurnal ensemble 30-minute averages of the surface radiation budget on the living roof of the California Academy of Sciences in San Francisco Ca.....	23
6. Per month diurnal ensemble averages of the surface radiation budget on the living roof of the California Academy of Sciences in San Francisco Ca, from April 2014 to March 2015.....	25
7. PAR diffuse with standard deviation and PAR global diurnal ensembles on the California Academy of Sciences Living Roof, San Francisco, Ca.....	26
8. Surface radiation budget terms (2014-2015) during clear and cloudy sky conditions, on the California Academy of Sciences Living Roof, San Francisco, Ca.....	26

9. Diurnal ensemble averages of the surface energy balance terms for the total study period (April 2014 – March 2015) on the California Academy of Sciences' living roof, San Francisco, Ca.....	30
10. Daily ensemble averages per month of the surface energy balance terms on the California Academy of Sciences' living roof, San Francisco, Ca. 2014-2015....	33
11. Surface energy balance 2014-2015 during clear and cloudy sky conditions, on the California Academy of Sciences Living Roof, San Francisco, Ca.....	34
12. Partitioned diurnal ensemble ground heat flux terms for October – December 2014, where Q_G is the total ground heat flux, Q_{G-15cm} is the ground heat flux measured at -15 cm, Q_{G-5cm} is the ground heat flux at -5cm, and $storage_{0-5cm}$ is the change in heat storage between -1 and -5 cm. Measured on the living roof of the California Academy of sciences, San Francisco, Ca.....	35
13. Seasonal variation in ground heat flux measurements on the living roof of the California Academy of Sciences, San Francisco, Ca, 2014.....	36
14. Daily ensemble averages of the surface shortwave radiation budget for the same three months in 2013 and 2014 on the living roof of the California Academy of Sciences in San Francisco Ca.....	38
15. Daily ensemble averages of the surface energy balance for the same three months in 2013 and 2014 on the living roof of the California Academy of Sciences in San Francisco Ca.....	40
16. Energy balance closure (April 2014 – March 2015) on the living roof of the California Academy of Sciences in San Francisco, CA.s Where low BR observations is Bowen < 1.3 and high BR observations is Bowen ratio > 1.3....	42
17. Energy balance closure (April 2014 – March 2015) on the living roof of the California Academy of Sciences in San Francisco, CA.s Where low BR observations is Bowen < 1.3 and high BR observations is Bowen ratio > 1.3.....	43

1.0 Background and Introduction

1.1 Urban climates and vegetation cover

Surface composition has a large potential to affect local climates. A number of studies have shown that vegetation in urban areas impacts the surface energy balance, hydrological cycle, and carbon budget (Honjo et al. 2003, Santamouris et al. 2007, Xu and Baldocchi 2004), particularly in urban settings, which are often categorized by warmer dryer climates when compared to surrounding landscapes. Urban areas tend to have high aerosol levels, and altered wind flow due to the complex nature of the built environment. These attributes combined with the material composition of city landscapes fosters an anthropogenic climate that differs substantially from rural landscapes. In this setting, vegetation can be an important tool in mitigating city climates so that they behave more similarly to that of natural ecosystems (Oke 1973). With their increasing geographic expansion, and growing populations, urban landscapes are becoming an increasingly dense anthropogenic biome (Alessa and Chapin 2008) with their own unique climate attributes. In 1990 less than 40% of the global population resided in urban dwellings, in 2010, over 50% of an even larger global population occupied city housing. By 2030, it is estimated that 60% of people will reside in cities (WHO 2013, Arnfield 2003). Therefore there is a need to better understand urban climates and how urban structure features impact the local climate. This study's data was collected between May of 2013 and March of 2015. The objective was to obtain a micrometeorological profile of living roof, specifically the roof's impact on the surface radiation budget and surface energy balance.

1.2 UHI and PCI

The first published observational study of urban climate was conducted in London by Luke Howard (Howard 1833, Oke 1980), who utilized thermometer based observations. The study demonstrated that London had a higher temperature than the surrounding countryside. However, it is worth noting that as early as the Roman Empire, scientists used visual observations of the urban atmosphere to suggest heat differences from surrounding rural areas, signifying urban climate effects (Grimmond 2006). This temperature difference is known as the urban heat island (UHI) effect, and can be expressed as:

$$UHI = T_{\text{urban}} - T_{\text{rural}} \quad (1)$$

where T_{urban} is the temperature within the city space, and T_{rural} is the temperature of the surrounding rural space. The built urban environment is comprised largely of asphalt, brick, glass, concrete, and steel. These urban construction materials contribute to localized high temperatures by their greater ability to store heat (Oke et al. 1991, Eliasson 2000). Heat storage capacity is particularly significant in cities when observed on a diurnal scale: often the largest difference in temperatures between urban and rural landscapes occurs in the early evening (Oke et al. 1991). Just as there is a temperature gradient between urban and rural spaces, there is similarly a temperature gradient between cities and urban parks. This phenomenon is known as the park cool island (PCI) effect, and expressed as:

$$PCI = T_{\text{urban}} - T_{\text{park}} \quad (2)$$

Where T_{park} is the temperature within the park. PCIs and UHIs have been observed in a range of climates and locations including in Hungary, Sweden, Japan, Singapore, Canada and United States (Bottyan et al. 2005, Homer and Eliasson 1999, Honjo et al.

2004, Susca et al. 2011). All studies on the phenomenon evinced the presence of PCIs and UHIs, (Honjo et al. 2004, Jansson et al. 2007, Spronken-Smith et al. 1998, Szegedi et al. 2009).

Different vegetation characteristics have different controls on park climate (Jansson et al. 2007, Spronken-Smith et al. 1998). Attributes such as the amount of open grass, tree height, leaf area index, and the presence of walkways or recreational facilities all impact the surface energy balance and hydrological cycle differently (Szegedi et al. 2009, Spronken-Smith et al. 1998). The structural components of the surrounding urban areas also play a role in urban PCI values. It has been observed that a structurally dense, and thus warm neighborhood, enhances the PCI whereas highly vegetated urban areas such as tree-lined streets reduce it. Shade, surface albedo, and the availability of water are all highly important controls on temperature during the daytime (Spronken-Smith et al. 1998). The sheer amount of vegetated vs. non-vegetated surfaces has an effect on PCIs. Weng et al. (2004) found that vegetation abundance is effective in adjusting land surface temperature.

1.3 Living roofs

Living roofs, also commonly referred to as “green roofs”, are roofs with a planted surface in their final structural layer (Berardi et al. 2014). While urban park spaces have been fairly well researched, the microclimate of living roofs is an understudied area of urban microclimatology. Roofs occupy up to 32% of the planimetric area of cities (Oberndorfer et al. 2007). Non-living roofs, which for the purpose of this study area defined as any roof without planted vegetation, are made up of the same heat-storing and heat-conducting materials that lead to the UHI phenomenon. Most non-living roof surfaces,

particularly in the commercial or industrial residential sector tend to be capped by concrete, gravel, or water resistant tar. In a 2008 study in Madrid comparing living roofs to gravel and white ones, the gravel roof had a solar absorption value of 0.8, compared to a living roof's solar absorption value of 0.37 (Saiz 2008), thus illustrating how standard roofs have the potential for a low albedo compared to certain vegetation coverage such as grasslands and succulent ecosystems (Weng et al. 2004, Saiz 2008). Because roofs offer such a large amount of unused urban space, they could represent a substantial cooling potential if converted to a living state.

Living roofs are not a new concept. The practice of installing substrate and planting vegetation on a rooftop has been in existence for centuries. As early as the 5th Century B.C.E., living roofs have been documented by cultures across Europe and Mesopotamia, with the Hanging Gardens of Babylon (in the current location of Syria) being widely attributed as the first recorded living roof (Williams et al. 2010, Oberndorfer et al. 2007). Romans historically employed living roofs as edible landscaping and for esthetic purposes, while the living roof was used as an architectural tool by Scandinavian countries (most notably Norway) for thermal insulation, a technique that is still employed in Scandinavia today (Berardi et al. 2014). In the 1970s there was a resurgence in developed countries to implement living roofs, not only for their insulative and aesthetic properties, but for their climatological benefits associated with the then emerging understanding of the UHI effect (Berardi et al. 2014). Since the 1970s studies have been conducted on the cooling capacity of living roofs both internally and externally, on their impact on the hydrological cycle, and their ability

to modify the partitioning of the urban energy balance (Berardi et al. 2014, Feng et al. 2010, Jim and He, 2010).

Most research conducted on living roofs is in the field of engineering, and involves their ability to insulate the building below and reduce heating and cooling costs. Two studies in Toronto, Canada and Ujjain, India compared the heat flow reduction and cooling properties of living roofs vs. nonliving ones. Both studies measured the temperature within the rooms below the living roofs and control roofs. In each study it was found that the temperature fluctuations and heat flow through the roof was reduced under living roof conditions, with Toronto exhibiting a 70-90% reduction of indoor temperature in summer and a 10-30% reduction in winter (Liu and Minor 2005, Pandey et al. 2013).

While living roofs have been shown to function well as insulators, a determining factor of the thermal capabilities of living roofs is the thermal resistance of the non-living roof below. If the living substrate sits atop a roof with substantial synthetic insulation, then the energy balance of the living roof would be decoupled from that of the roof below, thereby reducing the cooling-capacity of the roof as an insulator and creating a greater impact on the external outdoor micro-climate than the internal climate profile of the building (Berardi et al. 2014, Castleton et al. 2010, Jaffal et al. 2012).

Many studies treat living roofs as though they represent an additional layer of insulation with certain conductive properties (Berardi et al. 2014). The presence of vegetation however, accounts for additional cooling properties that differ from simple insulation. To understand the various cooling mechanisms of living roofs on both the

interior and exterior of buildings, it is necessary to evaluate the relative partitioning of heat fluxes in the surface energy balance.

1.4 The surface energy balance and radiation budget

The surface energy balance of a vegetated surface is expressed as:

$$QN = Q_E + Q_H + Q_G \quad (3)$$

where QN is net radiation, Q_E is the latent heat flux, Q_H is the sensible heat flux and Q_G is the ground heat flux. The surface energy balance is driven primarily by net radiation, which is comprised of the balance of four radiation components in two broad wavelength bands:

$$QN = KN + LN = K_{dn} - K_{up} + L_{dn} - L_{up} \quad (4)$$

Where KN is the net shortwave solar radiation, LN is the net longwave or thermal infrared radiation, K_{dn} and L_{dn} are the incoming shortwave and longwave radiation, and K_{up} and L_{up} are the outgoing shortwave and longwave radiation. The surface energy balance is partitioned differently depending on the ecosystem, as evidenced by numerous energy balance studies in ecosystems around the globe (Oliphant 2012). In theory, if there is no error in measurements, and no other terms are present, the component parts of the energy balance including sensible (Q_H), latent (Q_E) and ground heat (Q_G) combined will equal the net radiation (QN). (Arnfield 2003, Spronken-Smith et al. 2000, Masson et al. 2002). When dealing with a three dimensional surface environment such as urban or vegetated surfaces, the term ΔQ_s is often used to represent heat storage within this volume. Unlike Q_H and Q_E , ΔQ_s is not measured directly. Instead, a number of constituent components are used to estimate it, such as the ground heat flux and storage of heat within the vegetation or built environment as

well as latent and sensible heat storage fluxes within the column of air between the roughness elements, and the photosynthetic heat component (ΔQ_P) (Oliphant et al. 2004).

In urban areas, an additional term in the surface energy balance is the anthropogenic heat flux (Q_F) (Grimmond and Oke 1995). This is the heat that is created in large part by combustion, heating and cooling, and in small part by human metabolism. Q_F is typically substantially smaller when compared to net radiation for any given location. For example the diurnal maximum Q_F in a study conducted in Tokyo Japan was found to average consistently around 200 ($W m^{-2}$) in the summer compared with almost 800 ($W m^{-2}$) (measured at noon) of shortwave radiation (Ichinose et al. 1999).

Controls on the surface energy balance can include atmospheric demand, turbulent transport, surface resistance, water vapor transport, air temperature, soil water content (Wilson et al. 2002), available energy, canopy surface and aerodynamic conductance, atmospheric humidity deficit (Baldocchi et al. 1997), surface albedo, evapotranspiration, and land disturbance (Liu et al. 2005), building material, presence and retention of water, vegetation cover, and tree height (Szegedi et al. 2009, Spronken-Smith et al. 1998).

Latent heat would not be a dominant component of the surface energy balance of a non-living roof, unless for some reason there was ponding occurring. Therefore it can be hypothesized that a living roof would have a lower Bowen ratio (β) than a non-living roof. The Bowen ratio is a common method of evaluating the relative partitioning of the surface energy balance (Blad and Rosenberg 1973) (Equation 5).

$$\beta = Q_H/Q_E \quad (5)$$

2.0 Study Site

2.1. Location and background

The California Academy of Sciences (Cal Academy) is located within the eastern span of Golden Gate Park in San Francisco, California (Figure 1) located at 37.77°N, 122.48°W. San Francisco has a Mediterranean climate with average maximum and minimum summer temperatures between 15 C° and 21 C° and 10 C°, and 12 C° respectively, and winter average maximums and minimums between 12 C° and 15 C°, and 7 C° and 10 C° respectively (Null 1995). Golden Gate Park is a 412 ha mixed-use urban park (SF Parks and Rec 2014) that is buffered on 3 sides by neighborhoods. The Pacific Ocean borders the western edge of the park and prevailing winds are west, northwesterly (Null 1995). San Francisco's climate is characterized by dry summers, due to the migrating Pacific high pressure cell which deflects storms to the north, thus limiting summer precipitation. Conversely, in the winter, the high pressure cell loses intensity and moves southward, allowing for the intrusion of the moisture-laden low pressure cell, resulting in cool wet winters (Conomos et al. 1985). There is a frequent advection fog layer typically present in Golden Gate Park during summer (Oberlander 1956).

During this study period, San Francisco experienced a record-breaking drought. In 2013 San Francisco received 142 mm rainfall, compared to 647 mm in 2012, according to the NOAA weather station located in downtown San Francisco, roughly 15 km to the west of the study site. However the living roof was regularly irrigated at night using a surface sprinkler system. Therefore, the flora on the Cal Academy roof did not completely experience the climate region's typical summer dry-out, although there did

appear to be a visual decline in the vitality of some species during the summer compared to the onset of the project (Figure 2). According to the Cal Academy's senior botanist Frank Alameda, the reason for year-round irrigation of native plants that are ostensibly climate-tolerant, is to keep the roof in its most vibrant and esthetic state, thereby encouraging human interest and education (Cal Academy 2014).

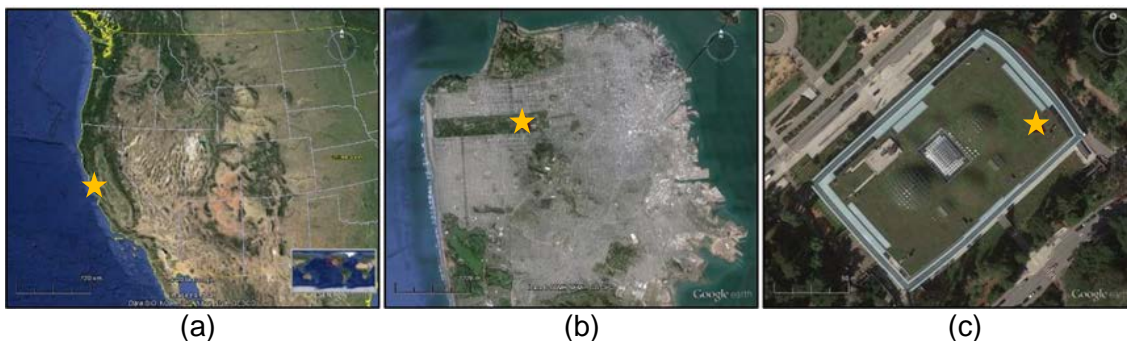


Figure 1. Location of the study tower (a) on the west coast of the US in the state of California (b), within the eastern span of the Golden Gate park in San Francisco and (c) on the southeast corner of the California Academy of Sciences' Living roof (Google Earth)

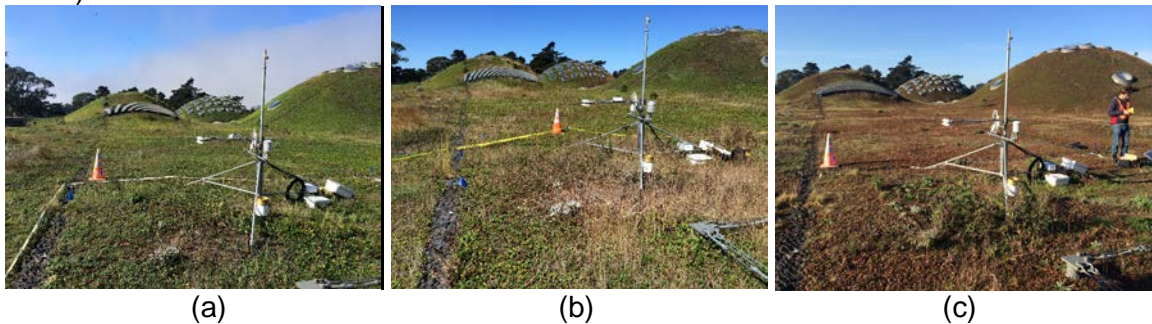


Figure 2. Visual evidence of seasonal variation in vegetation vitality on the California Academy of Sciences' living roof, in San Francisco Ca for the months of (a) May 2014, (b) August 2014 and (c) February 2015.

The Living roof was designed by architect Renzo Piano in conjunction with ecological designers Rana Creek, and sits atop a 4 story building located at 55 Music Concourse Dr., Golden Gate Park San Francisco, California (Figure 1). There are 3 major component roof features: living vegetation and bare soil, the concrete observation

deck and walkway, and the glass atrium and skylights (Figure 1c). The roof also has a number of vents, the most prominent of which are located in the northwest and southeast corners, as well as atop the smaller southeast dome. The roof has a unique topography, with 3 large multi meter domes, and 4 smaller domes situated around the central atrium.

There are 2 major classifications for living roofs: *intensive* and *extensive*. Living roof attributes that define these classifications are shown in Table 1.

Table 1. Classifications of living roofs (Berardi et al. 2014)

<i>Attribute</i>	<i>Extensive roof</i>	<i>Intensive roof</i>
<i>Thickness of growing media</i>	Below 200 mm	Above 200 mm
<i>Accessibility</i>	Inaccessible	Accessible
<i>Weight</i>	60-150 kg/m ²	Above 300 kg/m ²
<i>Diversity of plants</i>	Low	High
<i>Construction</i>	Moderate, easy	Technical, complex
<i>Irrigation</i>	Often not necessary	Necessity of drainage and irrigation systems
<i>Maintenance</i>	Simple	complex

Based on Berardi et al.'s definition, the California Academy of sciences is classified as an amalgamation of the two categories. As shown in Table 1, one factor in differentiating the two types of living roof classifications is substrate thickness. Despite being 5 cm short of the 20 cm substrate thickness that is often the marker of an intensive roof, the Cal Academy's roof can be classified as intensive due to its irrigation system, weight, relatively complex maintenance, accessibility and diversity of flora. On the other hand, one attribute of the Cal Academy's living roof that could be classified as extensive, was the size of the roof itself. Typically intensive roofs are much smaller than extensive ones. High plant species diversity is particularly utilized in classifying extensive vs intensive roofs. Species diversity also allowed for comparison between the Cal Academy

living roof and other similar ground level environments. A purely extensive roof, by comparison, such as the one in Wushan, Guangzhou, People's Republic of China used as a case study by Feng et al. (2010), had a very shallow substrate (4 cm), and a low diversity of flora; the only species of note being *sedum lineare*; making it a worthwhile comparison to the Cal Academy living roof, but difficult to compare to natural *landscapes*. Another study conducted by Theodosiou (2003) used a more intensive roof in Thessaloniki Greece with a substrate thickness of 12 cm; also comparable to the Cal Academy living roof.

2.2 Subsurface roof structure

The "living" component of the Cal Academy roof lies above a 6 layer roof system designed to provide drainage, contain soil, and insulate the building below. The living roof was constructed using 50,000 biodegradable husk trays made from coconut and sap, produced in the Philippines; these trays were then filled with soil and planted. Over time the coconut trays biodegraded and root systems interwove between adjacent trays creating a continuous vegetated surface. The original purpose of the planted tray technique was to find a way to stabilize sediment on the contoured domes (Cal Academy 2014). The roof is structured as follows: below the planted coconut trays (7.62 cm) there is an additional 7.62 cm of soil. Below the soil is an erosion control blanket designed to retain soil on the roof's slopes, retain moisture mid-slope, and control pest plants. A drainage layer to prevent plants from rotting is under the erosion control blanket, and below it is an insulation layer to stabilize internal building temperatures. Below that is a waterproofing layer, and finally there is a concrete slab that follows the

contours of the roof's seven hills (Cal Academy, 2014). This structure is similar to that of previously studied living roofs (Berardi et al. 2014, Feng et al. 2010, Jim and He, 2010).

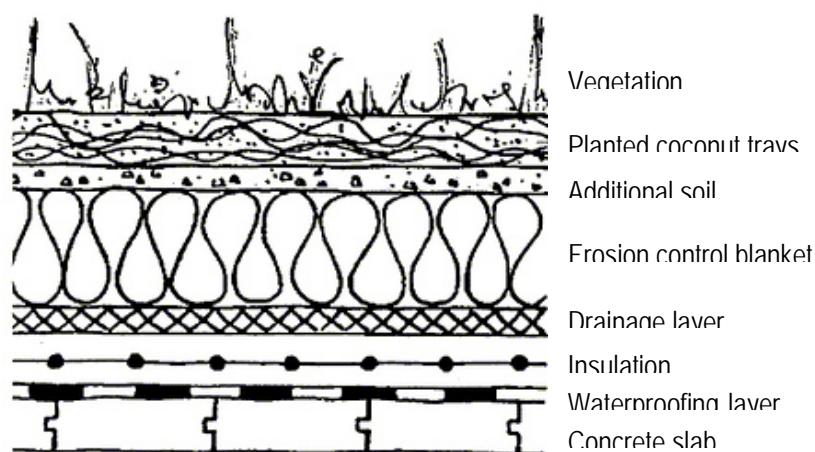


Figure 3. Schematic of the living roof structure on the California Academy of Sciences, San Francisco, Ca.

2.3 Ecology and vegetation surveys

Coastal chaparral and north coastal prairie are the two native California ecosystems that best categorize the Cal Academy living roof's flora. Coastal chaparral occupies 3,400,200 ha of California, and north coastal prairie encompasses 351,500 ha (Barbour et al. 1988). The Living roof's vegetation is a cross between the aforementioned ecosystems rather than simply a coastal chaparral ecosystem, because unlike much of the coastal chaparral that covers the surrounding Bay Area hillsides, the living roof has fewer shrubs and far more grass and wildflower species. Unlike either ecosystem in its natural state, the living roof is substantially manicured and weeded. The substrate of the Golden Gate Park is USGS soil type D, which includes some Quaternary muds, sands, gravels, and silts (USGS, 2012). The Cal Academy living roof's substrate is supplemented with compost and constructed with soil that best sustains the native plant species (Cal Academy, 2014).

The Cal Academy living roof was originally planted with 1.7 million individual plants of 9 native species (Cal Academy, 2014). Since construction completed in 2008, additional natives and non-natives alike have colonized the roof. In May and June of 2014, vegetation surveys were conducted to determine species diversity, relative cover, and canopy height. Employing a similar technique to that of Kalra (1996), the Cal Academy roof was broken into 49 m² sampling quadrants based on the existing rooftop grid pattern. The total area of the roof (including roof features) is roughly 10,241 m². Of this, the central atrium accounts for 5.74% (588 m²), the observation deck accounts for 2.87% (294 m²), and the other roof features such as cages, vents and skylights, combined together account for approximately 9.56% (980 m²). 124 sampling quadrants (6076 m²) met the criteria of being entirely vegetated with no major roof features, and having a flat or only slightly inclined surface. None of the 3 major domes were sampled due to access constraints. There were 41 additional vegetated, flat, partial quadrants that were not sampled due to irregular size.

A total of 22 sampling quadrants were utilized. These were geographically dispersed across the roof. 21 points were sampled in each sampling quadrant. A random-number table was used to generate stratified random sample points along 7 transects in each sampling quadrant (Figure 3). Beach strawberry (*fragaria chiloensis*) dominated the Cal Academy roof's vegetation profile with 32.9% coverage (Table 2). The next most common species occurrences were California bent grass (*Agrostis densiflora*) 11.8% and bare soil 8.8%. The average height of vegetation was 14.6 cm.



Figure 4. Researchers conducting point sampling for vegetation surveys on the living roof of the California Academy of Sciences, San Francisco Ca, 2014.

Table 2. List of plant species and percent cover of each on the living roof of the California Academy of Sciences in San Francisco Ca, 2014.

Plant species	Latin name	Observations	% cover
bare soil	NA	44	8.8%
beach strawberry	<i>Fragaria chiloensis</i> ,	164	32.9%
bur clover	<i>Medicago</i>	7	1.4%
California bent grass	<i>Agrostis densiflora</i>	59	11.8%
California fuchsia	<i>Epilobium canum</i>	6	1.2%
California poppy	<i>Eschscholzia californica</i>	1	0.2%
California sweet grass	<i>Hierochloe</i>	15	3.0%
coast dudleya	<i>Dudleya caespitosa</i>	1	0.2%
common yarrow	<i>Achillea millefolium</i>	28	5.6%
dandelion	<i>Taraxacum</i>	7	1.4%
fireweed	<i>Chamerion angustifolium</i>	17	3.4%
foxtail fescue	<i>Festuca</i>	35	7.0%
golden-eyed grass	<i>Sisyrinchium californicum</i>	8	1.6%
gumweed	<i>Grindelia</i>	10	2.0%
leaf litter	NA	16	3.2%
lupin	<i>Lupinus</i>	6	1.2%
nutgrass	<i>Cyperus rotundus</i>	8	1.6%
scorpionweed	<i>Phacelia</i>	10	2.0%
plantain weed	<i>Plantago major</i>	2	0.4%
purple needle grass	<i>Nassella pulchra</i>	2	0.4%
scouringrush horsetail	<i>Equisetum hyemale</i>	4	0.8%

seaside daisy	<i>Erigeron glaucus</i>	9	1.8%
seep monkeyflower	<i>Mimulus</i>	14	2.8%
self heal	<i>Prunella</i>	15	3.0%
sowthistle	<i>Sonchus</i>	7	1.4%
yellow primrose	<i>Primula vulgaris</i>	3	0.6%

3.0 Materials and Methods

3.1 Deployment

In summer 2013 and for the majority of 2014, observations were made of the surface radiation budget and surface energy balance. All instruments were either mounted on a tripod tower or buried in the roof's substrate (Table 3). For above ground measurements, a CSTAT3 three-dimensional sonic anemometer (Campbell Scientific, Logan Utah) and a Li-7500 fast response infrared gas analyzer (LI-COR, Lincoln Nebraska) were stationed at 1 m above the surface. At 1.2 m and 1.1 m respectively, a BF5 sunshine sensor for photosynthetically active radiation (PAR) (Delta-T Devices, Cambridge UK), a four component net radiometer (Campbell Scientific, Logan Utah), and an HMP45c thermistor/hygistor (Campbell Scientific, Logan Utah) were mounted. A TE525 rain gauge (Campbell Scientific, Logan Utah) was mounted just above the surface at 0.4 m. Within the roof's substrate, two HFP01 ground heat flux plates (Campbell Scientific, Logan Utah) were buried at -5 cm in depth, two CS107 thermistors (Campbell Scientific, Logan Utah) were buried at -15 cm and -3 cm respectively, a CS616 soil moisture probe (Campbell Scientific, Logan Utah) was inserted to measure the average between the surface and 15 cm of substrate, and four spatially averaging CS109 thermocouples (Campbell Scientific, Logan Utah) were inserted between -1 and -5 cm to measure temperature above the ground heat flux plates. Power for all instruments was supplied

by multiple 12 V deep cycle batteries charged by a 75 W solar panel. All data were collected and stored in a CR3000 data logger in raw 10 Hz samples as well as 30 min averages. The gas analyzer was periodically calibrated using zero and span gasses for CO₂ and H₂O absorption calibration. On September 24th one of the two ground heat flux plates was moved and reburied at a depth of -15 cm.

Table 3. Biomicrometeorological instruments deployed on the California Academy of Sciences' living roof, San Francisco Ca, 2013-2015.

Equipment	Variable	Unit	Height/Depth	Frequency
HMP45c Thermistor	Temperature, relative humidity	C°	109 cm	10 Hz, 5 & 30 min averages
NR01 Pyranometer	Shortwave radiation	W m ²	110 cm	
NR01 Pyrgeometer	Longwave radiation	W m ²	110 cm	
BF5 Sunshine Sensor	photosynthetically-active radiation		119 cm	
CSAT3 3-D Sonic Anemometer	Spatial wind velocity, sonic temperature	m/s	108 cm	10 Hz, 30 min averages
Li-7500A Infrared Gas Analyzer	Humidity, Co ₂	%, mg/m ³	108 cm	
CS107 Ground thermistors	Temperature	C°	-3 cm & -15 cm	10 Hz, 5 & 30 min averages
HFP01 Ground heat flux plates	Heat flux	W m ²	-5 cm (-15 cm 09/14)	
CS109 Thermocouples	Temperature	C°	-1 cm & -5 cm	
CS616 Soil moisture probe	Soil moisture content	%	-15 cm	
TE525 Tipping Bucket Rain	Precipitation/irrigation	mm	47 cm	30-minute totals
2420-BLX-100 load cell	Evapotranspiration	mg	-15 cm	Every 5 S, 30 min averages

The eddy covariance technique was used to determine surface-atmosphere exchanges of carbon, water and heat energy. The eddy covariance technique measures

rates of vertical transport of atmospheric scalars by turbulent eddies - areas of upward and downward moving air - that transport the scalar of interest (Baldocchi et al. 2003). Eddy covariance is an established technique in the micrometeorological community and has been employed using the same or similar equipment at over 500 sites throughout the globe as part of the FLUXNET network (Oliphant 2012). The formula for eddy covariance can be written as:

$$F_s \approx \overline{\rho_a w' s'} \quad (6)$$

where F_s is the measured fluxes, ρ_a is the density of air parcel (which is considered to be a constant), w' is the fluctuations in the vertical wind velocity and s' is the scalar. The overbar denotes the time average of the instantaneous covariance of w and s (Oke 1987). This formula employs the concept that vertical fluxes of atmospheric scalars such as heat energy and trace gasses between the vegetated surface and the overlying atmosphere are proportional to the mean covariance between fluctuations of vertical velocities and the respective scalar (Wilson et al. 2002). Benefits of the eddy covariance technique include precise, high-frequency measurements, the ability to measure large swaths of land from a single station, and robust long-term data acquisition. Downsides include the inability to accurately measure non-homogeneous surfaces and the propensity to underestimate the turbulent fluxes.

3.2 Project footprint

A few site specifications had to be met in order to use eddy covariance; the first is concerning the fetch (the length of surface over which a given wind has blown). Eddy covariance derives data from a footprint that varies depending on the height of the equipment, as well as wind speed, surface roughness and atmospheric stability (Wilson

et al. 2002, Baldocchi et al. 2003), this makes stationing the instruments at a height representative of the source area crucial to measuring the desired area and nothing beyond. The fetch also fluctuates based on whether measurements are being made during stable or unstable conditions. To maximize usable data, the eddy covariance tower was installed as low as possible to the Cal Academy's roof's surface resulting in an average 80th percentile fetch distance that just passed the roof's atrium. By comparison, most eddy covariance towers established in previous studies are placed several meters high for shorter canopies, and over 10 m high for tall forests (Wilson et al. 2002).

The project footprint model was established from a data set acquired during a preliminary short-term study performed at the same location in summer 2013. In this study Hsieh et al.'s (2000) analytical footprint model was employed to estimate the project footprint for every 30 min interval. All periods when the 80th percentile of the cumulative flux distance fell outside of the roof area were rejected. The tower was installed in the southeast corner of the Cal Academy roof in order to obtain the largest rooftop footprint in the prevailing westerly wind direction. The Cal Academy has the only living roof in California large enough to utilize this technique, making this the premier study of living roofs using eddy covariance.

The second specification that had to be met in order to use eddy covariance is surface homogeneity so that advection (Q_A) can be discounted (Wofsy et al. 1993; Moncrieff et al. 1997), as any advection in this case would likely originate from outside the roof perimeter. The Cal Academy roof is complex. While the plant species and height distribution across the roof is fairly homogenous, the roof topography may cause local area flux deviations. The atrium center within the domes is the most significant roof

feature within the project footprint; it is typically opened at the end of the day to allow for cool air to drain down the domes into the plaza for interior cooling (Cal Academy 2014). The equipment was located roughly 15 m from the leeward edge of the building to avoid influence of vertical wind motions associated with the building edge. The anthropogenic heat flux was not independently measured in this study, as the only potential sources – vents and people on the observation deck – were largely outside the project footprint.

The various surface energy balance terms have unique controls depending on the environment. Latent heat (Q_E) and sensible heat (Q_H) fluxes were measured using the eddy covariance technique, while conductive ground heat (Q_G) is measured using ground heat flux plates. The equation for sensible and latent heat are as follows:

$$Q_E = \overline{L_v W' P_v'} \quad (7.1)$$

$$Q_H = \overline{C_a W' T'} \quad (7.2)$$

Where Equation 7.1 is the latent heat flux, where L_v is the latent heat of vaporization, W' is the fluctuations in vertical velocity and P_v is the vapor density of air, and Equation 7.2 is the sensible heat flux, where C_a is the specific heat of air, W' is the fluctuations in vertical velocity, and T' is the fluctuations in air temperature.

3.3 Determining the ground heat flux

Ground heat flux (Q_G) was determined using the two HFP01 ground heat flux plates buried at -5 cm, with CS109 thermocouples inserted above the plates and below the substrate surface to acquire temperature changes in the layer above the heat flux plates.

The derivation for Q_G here was:

$$Q_G = Q_{G(-5 \text{ cm})} + C_s \frac{\Delta t_{-1-5 \text{ cm}}}{\Delta t} \quad (8)$$

where $Q_{g(-5\text{ cm})}$ is the measured soil heat flux at depth -5 cm, C_s is the soil heat capacity, and t is time (Oliphant et al. 2011). Heat flux plates were buried to prevent solar radiation loading. The deeper the plates are buried, the less directly they measure the transfer of energy from the surface through the ground due to the storage medium between the flux plates and biosurface (Oke 1987). In order to account for this storage term, T-type averaging thermocouples were installed between -5 and 0 cm to capture the temperature in this small volume of soil. C_s was then derived from:

$$C_s = C_{\text{min}} + C_{\text{org}} + C_w + C_a \quad (9)$$

where C_{min} is the volume fraction of soil occupied by minerals, C_{org} is occupied by organic material, C_w is occupied by water, and C_a is occupied by air (de Vries 1963). In order to accurately calculate C_s , the component parts of mineral and organic content of the below ground soil were determined through analysis of soil samples. The soil and root structure were separated from the above ground organic content and dried in an oven at 80°C for approximately 7-24 hours to remove the weight of the water component. The samples were subsequently heated in a furnace at 360 °C for 2 hours to remove the organic content weight, leaving only the mineral component. The mineral fraction of the dry soil samples averaged 0.68, and the organic content was 0.32 with a standard deviation of 0.13. In order to calculate the bulk density of the soil, 6 150 cm³ soil tins were filled with substrate taken from between -14.5 and -7 cm, and between -7 cm and the surface. The samples were then dried in an oven at 80°C until the water component was removed. The average dry weight was 121 g, making the bulk density 0.81 g/cm³. For the purpose of this study, the storage term within the vegetated canopy

was considered negligible due to the average height of the canopy layer (14.6 cm) and this term was represented solely by the ground heat flux (Q_G).

On September 14, 2014, one of the ground heat flux plates buried at -5 cm was removed and re-buried at -15cm in order to determine the total amount of heat transferred through the entire substrate into the building roof below. During this period, the both heat flux plates took measurements at 10 Hz, and data was aggregated into 5 & 30 min averages.

4.0 Results

Data collected between May and July of 2013, and between March of 2014 and March of 2015 was analyzed to determine the characteristics of the surface radiation budget and the surface energy balance on the California Academy's living roof. Due to the high rate of data rejection (~50%) for eddy covariance terms, these characteristics were consolidated into 30-minute statistics for timeframes ranging from monthly to annual. These diurnal ensembles were derived using periods when all surface radiation budget and energy balance terms were available.

A full year of data was collected between 2014 and 2015; showing the annual variability of the living roof's microclimate. In addition, the summer deployment in 2013 allowed for inter-annual comparison of summer months between 2013 and 2014. Seasonal controls on the surface radiation and energy balance terms were examined; and energy balance closure was assessed on both a total study period and monthly time scale. The ground heat flux was analyzed at both at the soil-air and soil-roof interfaces to investigate conductive heat transfer into and out of the building roof.

4.1 Surface radiation budget

The diurnal ensemble averages for the components of the Surface radiation budget during the study period are shown in Figure 5. Incoming shortwave radiation (K_{dn}) peaked in the afternoon between 12:00 and 14:00 PST. The albedo of the living roof averaged 20% and was fairly consistent throughout the daylight period. As a result, an average of $13.18 \text{ (MJ m}^{-2} \text{ dy}^{-1})$ was absorbed by the living roof (Table 4). Seasonal variation in K_{dn} was primarily driven by solar declination and changes in cloud cover as evidenced by the low K_{dn} observations under cloudy conditions and high observations under clear sky conditions (Figure 8) as well as the corresponding high and low seasonal K_{dn} observations shown in Figure 6 during times of high and low solar declination. Due to the presence of summer advection fog, the peak in K_{dn} occurred in May, while July and August showed the most reduction due to cloud cover.

The albedo of the living roof had a seasonal range (4.9%), with highest observations occurring in the winter and spring, and then decreasing in the summer and early fall. This corresponds closely to the annual growth cycle of this Mediterranean ecosystem, with maximum foliage appearing in the wetter growing season over the winter and spring, and plant species drying out and dying off in the summer despite irrigation (Figure 2).

Incoming longwave radiation (L_{dn}) remained relatively constant throughout the diurnal cycle, reflecting the low diurnal air temperature range (Figure 5). There was also relative constancy in longwave radiation seasonally across months, indicating a low annual temperature range. The largest impact on L_{dn} is due to the presence or absence of clouds. Outgoing longwave radiation (L_{up}) was only slightly greater than L_{dn} , and

increased by $100.9 \text{ (W m}^{-2}\text{)}$ during the peak daylight hours, indicating the small temperature gradient between the surface and the atmosphere. Net radiation (QN) was strongly positive during the day, reaching an average maximum of $498.5 \text{ (W m}^{-2}\text{)}$, and weakly negative at night, with an average minimum of $-46.3 \text{ (W m}^{-2}\text{)}$. The average total values for the study period (in $\text{MJ m}^{-2} \text{ dy}^{-1}$) can be seen in Table 4. QN decreased significantly in the winter months due to solar declination, although its ratio to the other energy balance terms remained relatively constant over time.

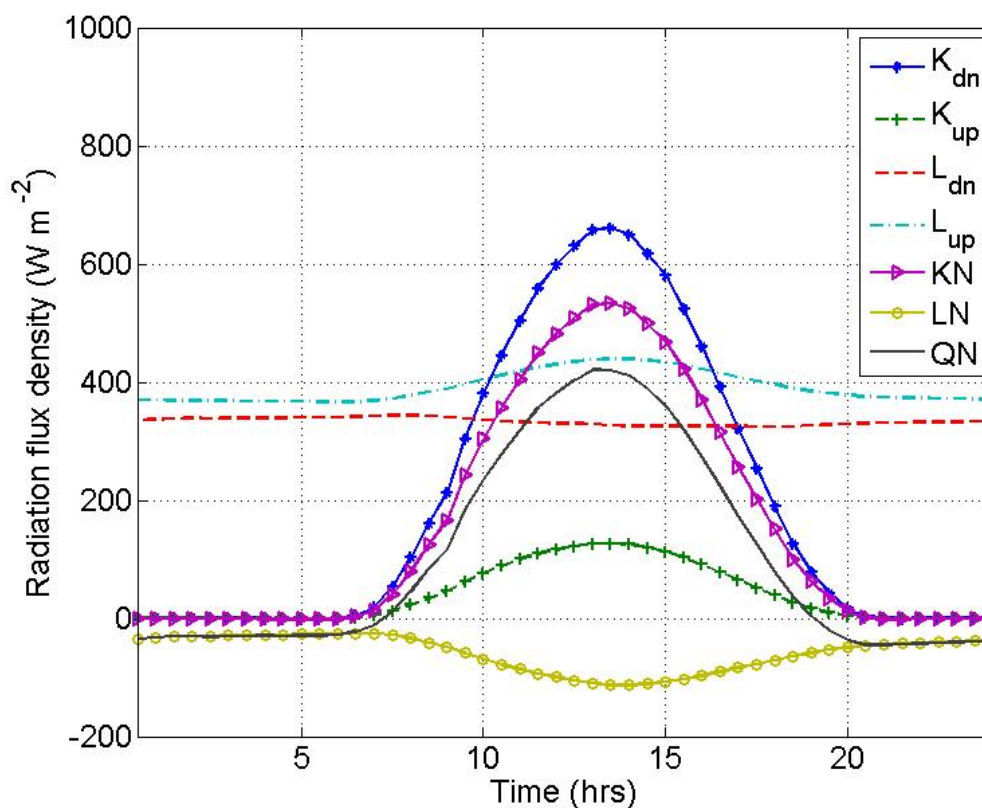


Figure 5. April 2014 – March 2015 diurnal ensemble 30-minute averages of the surface radiation budget on the living roof of the California Academy of Sciences in San Francisco Ca.

Table 4. Total study period and monthly totals (in $\text{MJ m}^{-2} \text{ dy}^{-1}$) for the component parts of the surface radiation budget. Measured on the living roof of the California Academy of Sciences, San Francisco, Ca, 2014-15.

	(K _{dn})	(K _{up})	(L _{dn})	(L _{up})	(KN)	(LN)	(QN)	(α)
	(MJ m ⁻² dy ⁻¹)							(%)
Total	16.52	3.34	27.97	33.71	13.18	-5.74	8.38	20.43
1_Jan	10.55	2.31	15.43	32.11	8.24	-16.7	2.82	21.90
2_Feb	14.68	3.10	25.99	32.41	11.58	-6.42	5.16	21.12
3_March	16.73	3.75	27.54	32.65	12.98	-5.11	7.87	20.84
4_April	21.70	4.85	27.57	33.19	16.85	-5.62	11.24	22.33
5_May	26.08	5.26	27.37	34.36	20.82	-5.99	13.83	20.16
6_June	24.97	4.66	29.07	34.64	20.31	-5.57	14.74	18.66
7_July	20.23	3.52	31.75	35.01	16.71	-3.26	13.45	17.39
8_Aug	15.23	2.77	32.10	34.45	12.45	-2.35	10.10	18.22
9_Sept	17.49	3.57	30.86	35.04	13.93	-4.18	9.74	20.39
10_Oct	13.95	2.95	29.75	34.54	11.00	-4.79	6.20	21.16
11_Nov	9.10	1.97	28.51	32.91	7.13	-4.4	2.73	21.65
12_Dec	6.62	1.41	30.41	32.70	5.21	-2.29	2.92	21.30

Figure 6 shows diurnal ensemble averages of the surface radiation at monthly timesteps. May had the greatest K_{dn} with peak values over 900 ($W m^{-2}$), followed closely by June and April, both of which peaked over 800 ($W m^{-2}$). With the summer solstice occurring on June 21st, it would then be assumed that June would have the highest K_{dn} values followed by July due to the solar declination. However, the fact that K_{dn} in June was lower than May, and July was lower than April suggests that summer cloud cover

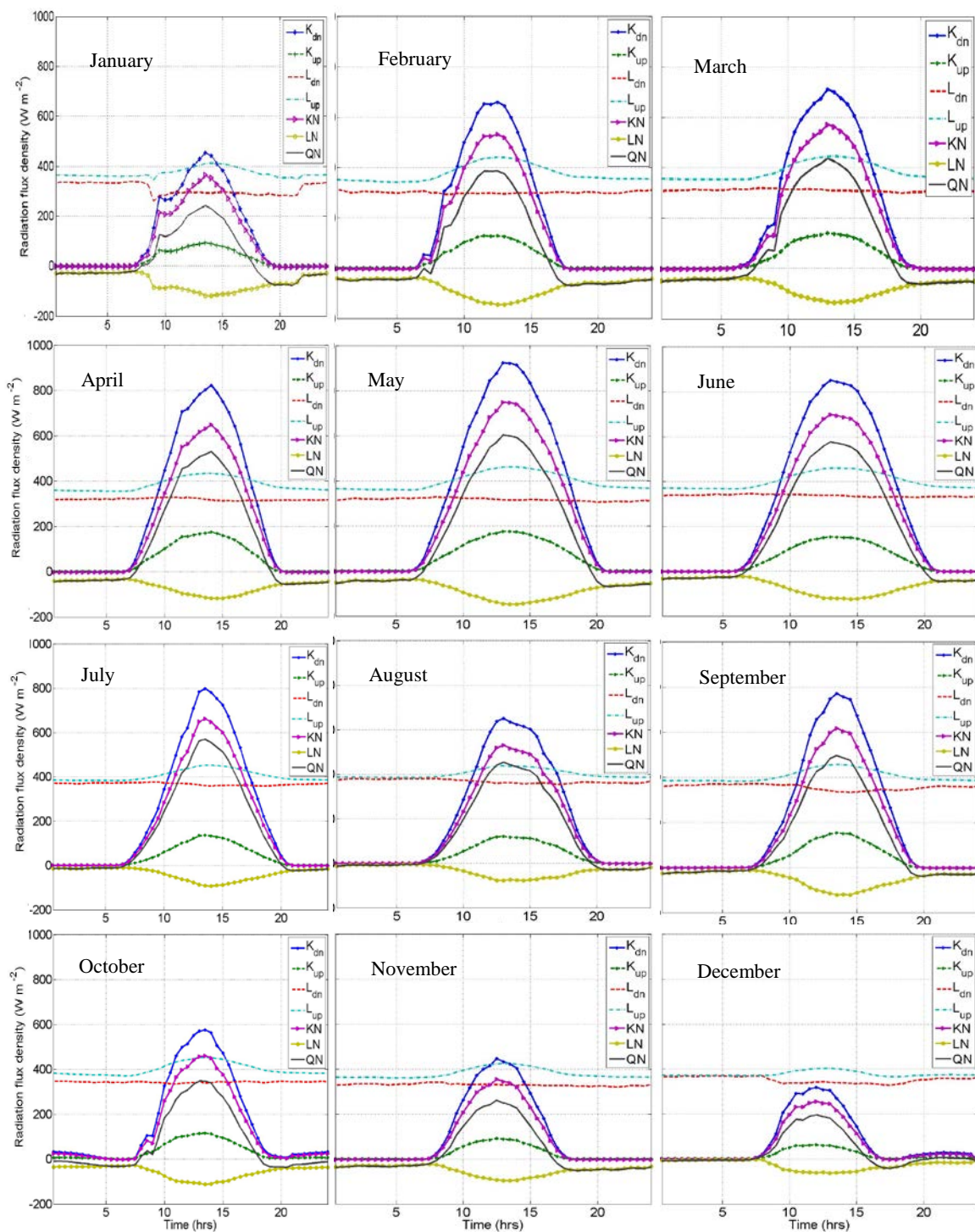


Figure 6. Per month diurnal ensemble averages of the surface radiation budget on the living roof of the California Academy of Sciences in San Francisco Ca, from April 2014 to March 2015.

due to advection fog strongly modified the effect of declination. The impact of cloud cover on the surface radiation budget is also evidenced by the amount of diffuse PAR occurring on a seasonal basis (Figure 7).

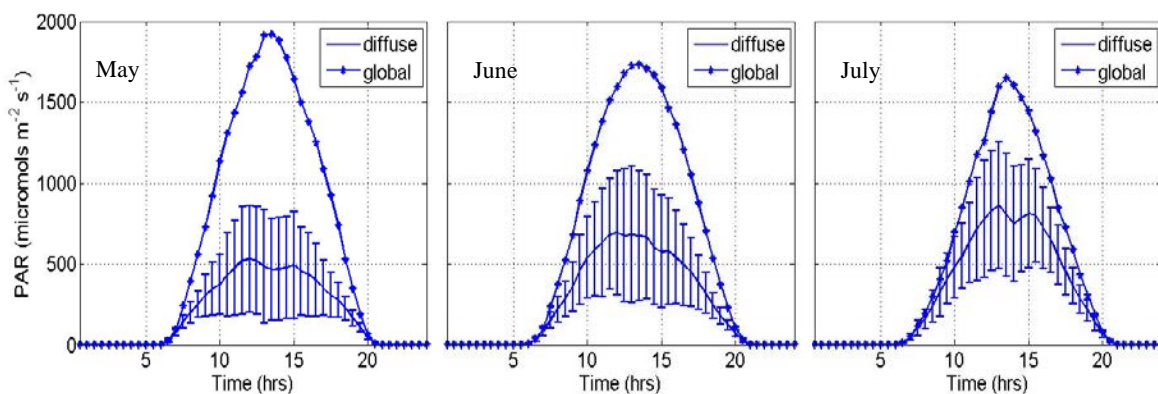


Figure 7. PAR diffuse with standard deviation and PAR global diurnal ensembles on the California Academy of Sciences Living Roof, San Francisco, Ca.

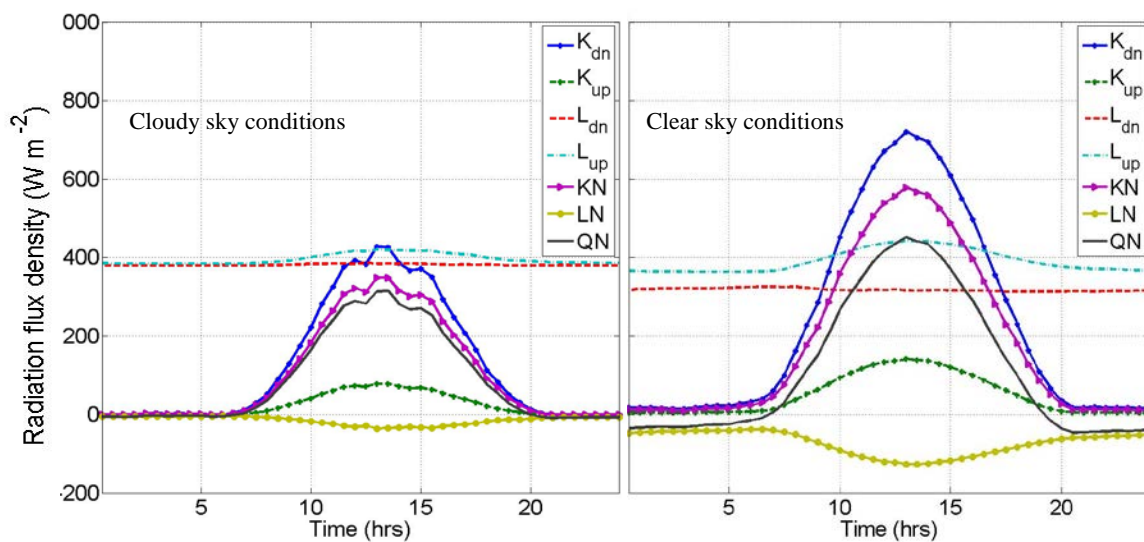


Figure 8. Surface radiation budget terms (2014-2015) during clear and cloudy sky conditions, on the California Academy of Sciences Living Roof, San Francisco, Ca.

Clear skies were defined as any time when L_{dn} was less than $370 \text{ (W m}^{-2}\text{)}$, and cloudy skies any time when L_{dn} was greater than $370 \text{ (W m}^{-2}\text{)}$ (Brant et al. 2008). Clear skies showed a smaller disparity between incoming and outgoing long wave radiation; both stayed consistent around $400 \text{ (W m}^{-2}\text{)}$ with a small increase during the day, whereas under clear skies, L_{dn} was noticeably lower than both the corresponding clear skies L_{up} , and the L_{dn} values under cloudy skies. This demonstrates clouds ability to reflect and in essence “trap” Longwave radiation.

4.2 Surface energy balance

In addition to directly measuring the component parts of the surface energy balance, the general meteorological climate conditions on the roof were measured to better understand environmental controls on the surface energy balance (Table 5). The Cal Academy roof’s precipitation followed the general trends for northern California with more rain events occurring in the winter and spring, followed by dry summer and fall seasons. The total amount of accumulated rainfall of 492 mm was greatly influenced by winter and spring rainfall. Inconsistent irrigation and sporadic rain events led to a large range (210 mm) of total precipitation values per month. December was the wettest month due to winter storms, but was followed by a record-breaking dry January. Still the levels of precipitation in the winter far outpaced the irrigation of the summer. Fall saw less irrigation and had a typically dry natural profile, making it the driest season for total precipitation despite January and February receiving the lowest individual precipitations values out of the year. The ratio of soil volumetric water content (VWC) to precipitation was not consistent across months.

Table 5. General monthly meteorological conditions between April 2014 and March 2015 on the California Academy of Sciences’ living roof, San Francisco, Ca.

	<i>Total precipitation/irrigation (mm)</i>	<i>Mean soil temperature (°C)</i>	<i>Mean volumetric water content (%)</i>	<i>Mean air temperature (°C)</i>	<i>Mean wind speed (mph)</i>
<i>Study period</i>	492	15.8	18.3	14.2	1.8
<i>1_Jan</i>	7	11.1	25	14.1	1.2
<i>2_Feb</i>	9	13.5	31	13.4	1.2
<i>3_March</i>	13	14.8	14	12.8	1.4
<i>4_April</i>	47	15.3	13	12.5	1.8
<i>5_May</i>	34	17.4	6	13.9	2.1
<i>6_June</i>	27	17.7	5	13.4	2.4
<i>7_July</i>	40	18.8	11	15.3	2.3
<i>8_Aug</i>	21	18.1	20	15.4	2.3
<i>9_Sept</i>	28	18.7	16	16.0	1.9
<i>10_Oct</i>	16	16.9	23	16.7	1.6
<i>11_Nov</i>	33	13.8	25	14.0	1.0
<i>12_Dec</i>	217	13.4	31	12.9	1.6

Figure 9 shows that the convective terms (Q_H and Q_E) dominated the partitioning of available energy (Q_N) during daylight hours. On an hourly basis they followed a similar trajectory to Q_N , with Q_H dominating when Q_N was high (from about 10am to 6 pm), while Q_E was higher in the first hours of daylight. At night, Q_H remained near zero, while Q_E was weakly positive throughout the night on average. Q_H had a time lag of roughly one hour compared to Q_N . Q_G was the last term to register daylight heating, and likewise followed a similar pattern as the other terms, but represented the smallest amount of partitioned energy (~10% of Q_N).

Q_H became negative at night, with a lowest value of -10.5 ($W\ m^{-2}$), while Q_E , only produced positive values for the averaged study period, with 10.5 ($W\ m^{-2}$) being the lowest recorded ensemble nighttime value. The relatively even partitioning of energy

between the turbulent heat fluxes resulted in a study period Bowen ratio (β) value of 0.96 (Table 6). Seasonally, Q_G remained consistently negative throughout the year, indicating that the building under the substrate was conducting heat outwards through the substrate into the atmosphere. The negative observations show how having a planted surface above a building differ from natural ecosystems where there would be no sub-surface heat source.

As Figure 10 shows, the latent heat flux began to surpass the sensible heat flux in October at the onset of the rainy season. Seasonally both convective fluxes were highest in summer, began to decline in the fall, and were reduced to less than half their summer values during the winter when all the energy balance terms were greatly reduced by the lack of incoming solar radiation. The seasonal variability shows how strongly the surface energy balance is driven by the magnitudes of the surface radiation budget, which was likewise dramatically reduced during the winter months.

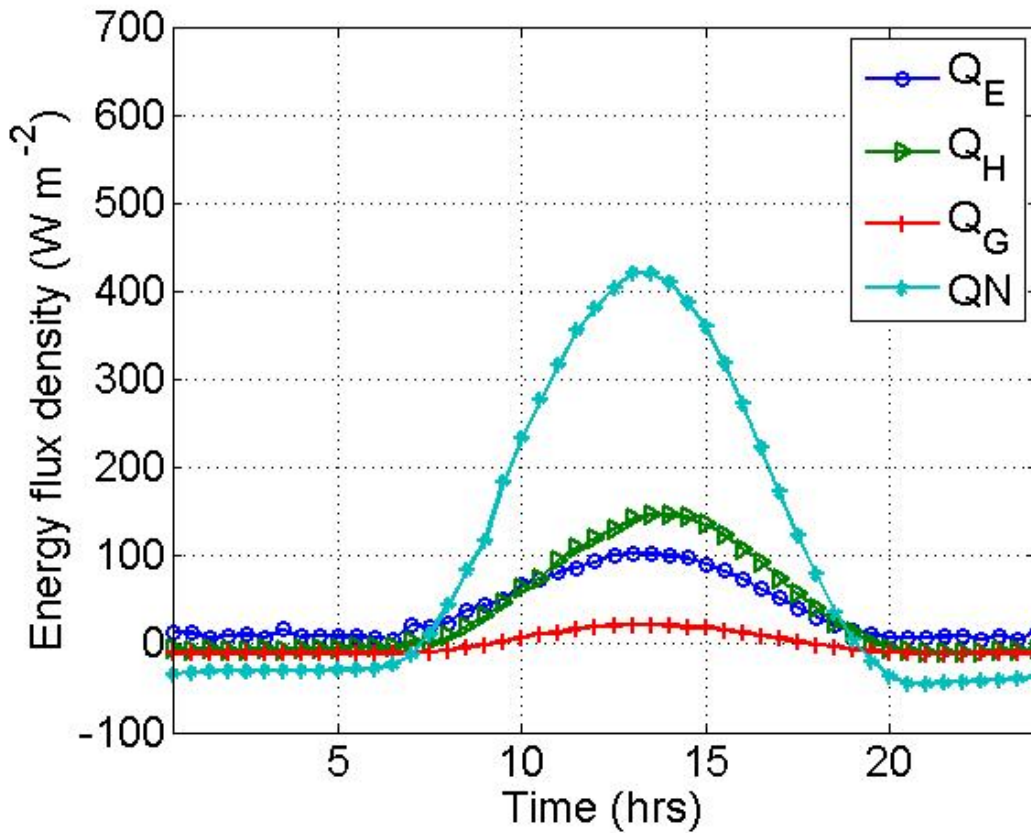


Figure 9. Diurnal ensemble averages of the surface energy balance terms for the total study period (April 2014 – March 2015) on the California Academy of Sciences' living roof, San Francisco, Ca.

Table 6. Total study period and monthly total values of energy balance terms as well as the Bowen ratio and residual (in $\text{MJ m}^{-2} \text{dy}^{-1}$). Measured on the living roof of the California Academy of sciences, San Francisco, Ca.

	QN	Q _E	Q _H	Q _G	(β)	Residual
	($\text{MJ m}^{-2} \text{dy}^{-1}$)					
Total	8.14	3.19	3.09	-0.07	0.96	2.20
1_Jan	2.82	1.03	2.13	-0.15	1.19	0.71

2_Feb	5.21	3.11	1.71	-0.09	0.55	0.47
3_March	7.66	3.75	2.64	-0.05	0.70	1.53
4_April	11.24	4.27	4.14	-0.04	0.97	2.87
5_May	13.83	4.74	5.20	-0.05	1.10	3.94
6_June	14.74	3.54	6.41	-0.01	1.81	4.81
7_July	13.45	3.82	5.19	-0.04	1.36	4.48
8_Aug	10.10	3.88	3.54	-0.03	0.91	2.71
9_Sept	9.75	3.53	3.52	-0.04	1.00	2.73
10_Oct	6.20	3.51	1.86	-0.02	0.53	0.85
11_Nov	2.74	2.31	0.82	-0.12	0.35	-0.27
12_Dec	2.95	0.81	0.81	-0.18	1.00	1.15

4.3 Controls on the surface energy balance

Controls on the surface energy balance were expected to include air and soil temperature, available energy, precipitation and VWC, and plant transpiration (Wilson et al. 2002, Liu et al. 2005). For the purpose of this study “precipitation” was defined as any measureable rainfall or irrigation water as measured by the TE525 tipping bucket rain gauge. Precipitation observations were only weakly correlated with Q_E ; with July and August having similar Q_E observations despite August receiving only half the precipitation of July (Tables 5 and 6). As previously noted, there was not a strong relationship between precipitation and VWC. Likewise there was not a strong relationship between Q_E and VWC; with Q_E being highest in April and May, and May having less than half the mean VWC of April. Q_H was highest in the summer months

(June, July and August) which corresponded to the highest mean wind speeds, although two of the summer months also had the highest residuals, it is unlikely that high mean wind speed is responsible for this, because July and August had the same exact mean wind speed, but vastly different residuals. Also winds speeds were likely driven by macro seasonal variations in onshore breezes from the western coast of San Francisco. Available energy was the strongest driver of the turbulent heat fluxes, as clearly evidenced by Figures 6 and 10.

Clouds also controlled the surface energy balance. Under clear sky conditions mean QN was $9.78 \text{ (MJ m}^{-2} \text{ dy}^{-1}\text{)}$, and was $7.55 \text{ (MJ m}^{-2} \text{ dy}^{-1}\text{)}$ under cloudy sky conditions. The Bowen ratio was 0.82 under sunny skies and 1.06 under cloudy conditions. This implies that there was greater evapotranspiration under clear skies (Figure 11).

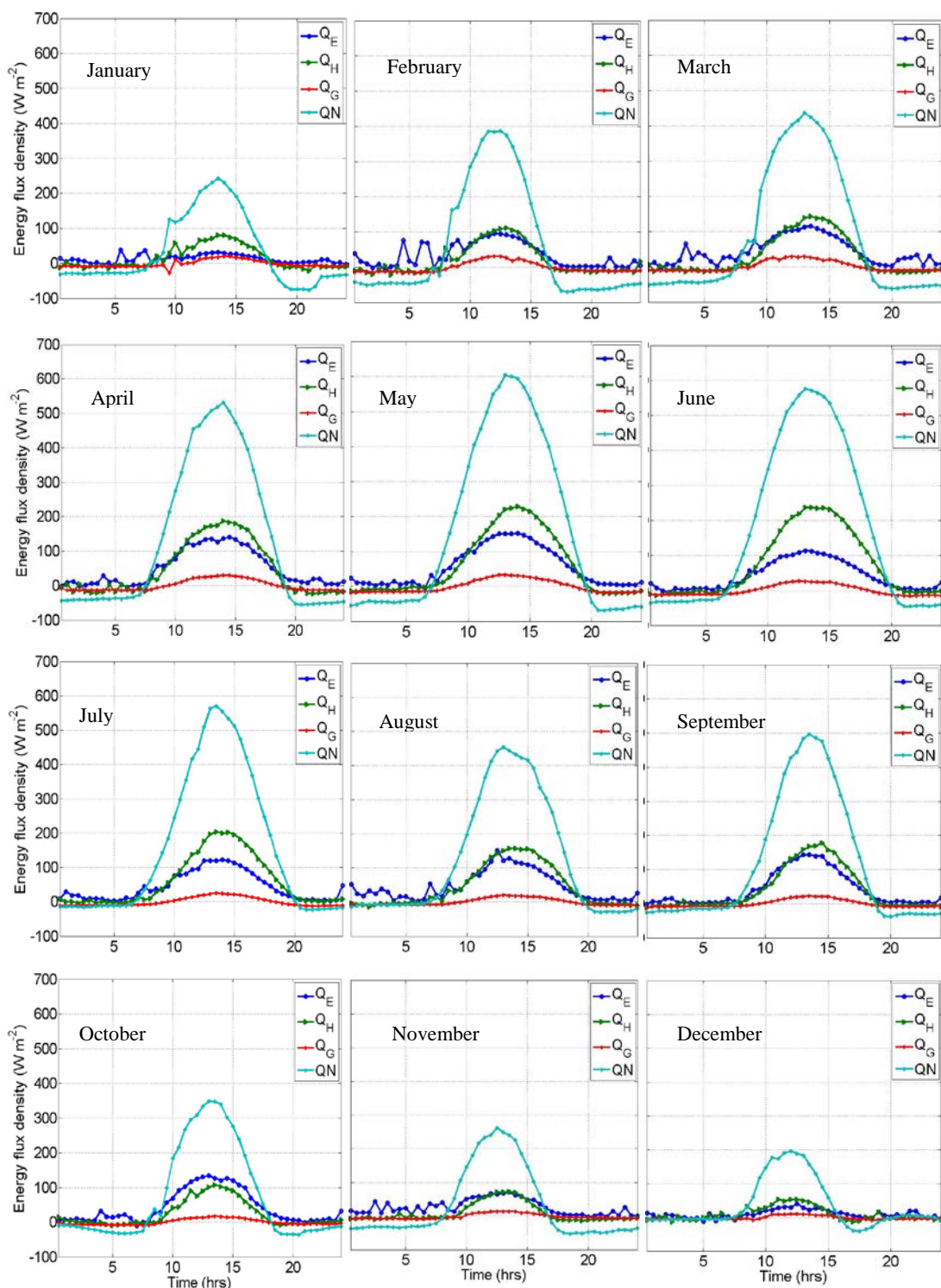


Figure 10. Daily ensemble averages per month of the surface energy balance terms on the California Academy of Sciences' living roof, San Francisco, Ca. 2014-2015.

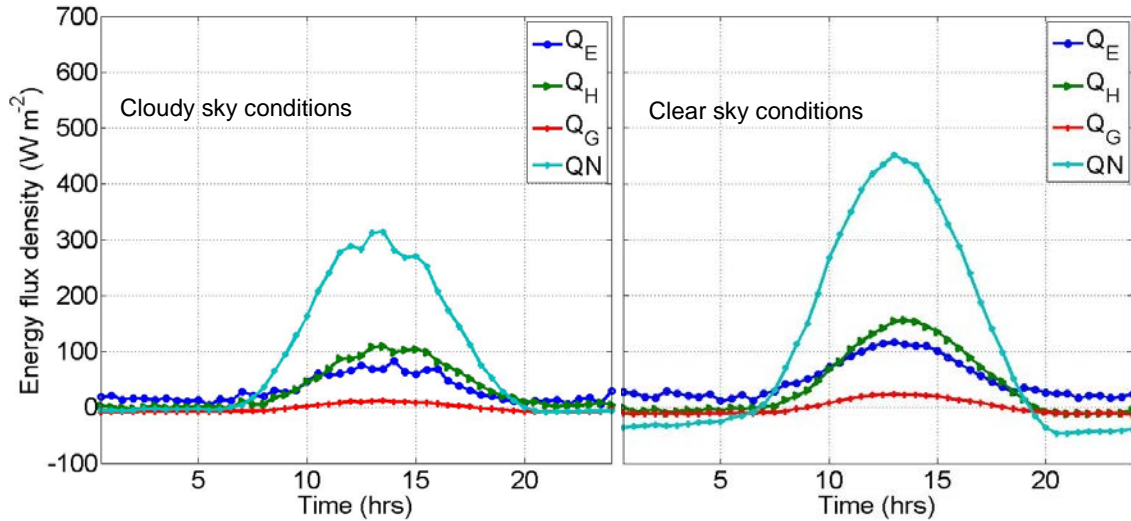


Figure 11. Surface energy balance 2014-2015 during clear and cloudy sky conditions, on the California Academy of Sciences Living Roof, San Francisco, Ca.

4.4 Ground heat flux

The ground heat flux followed the diurnal pattern of Q_N; Q_G responded quickly once the surface energy balance became positive at the onset of morning (Figure 12), first by predominantly heating the 0-5 cm layer of substrate, followed by conduction to deeper layers of the substrate/roof. In the afternoon the surface layer began to cool, despite a positive (downward) heat flux still at 5 cm. This reduced the overall ground heat flux at the surface until it became negative close to the evening sign reversal of Q_N. Q_G stayed weekly negative throughout the night. Over daily time periods, mean Q_G was also weekly negative for all months of the study period as seen in Table 6. This indicates a small net loss of heat from the building on an annual basis. Over the study period, the total ground heat flux was -0.07 (MJ m⁻²dy⁻¹). Both the ground and sensible heat fluxes

reached their peaks with more similar timing to one another than with the latent heat which peaked earlier in the day.

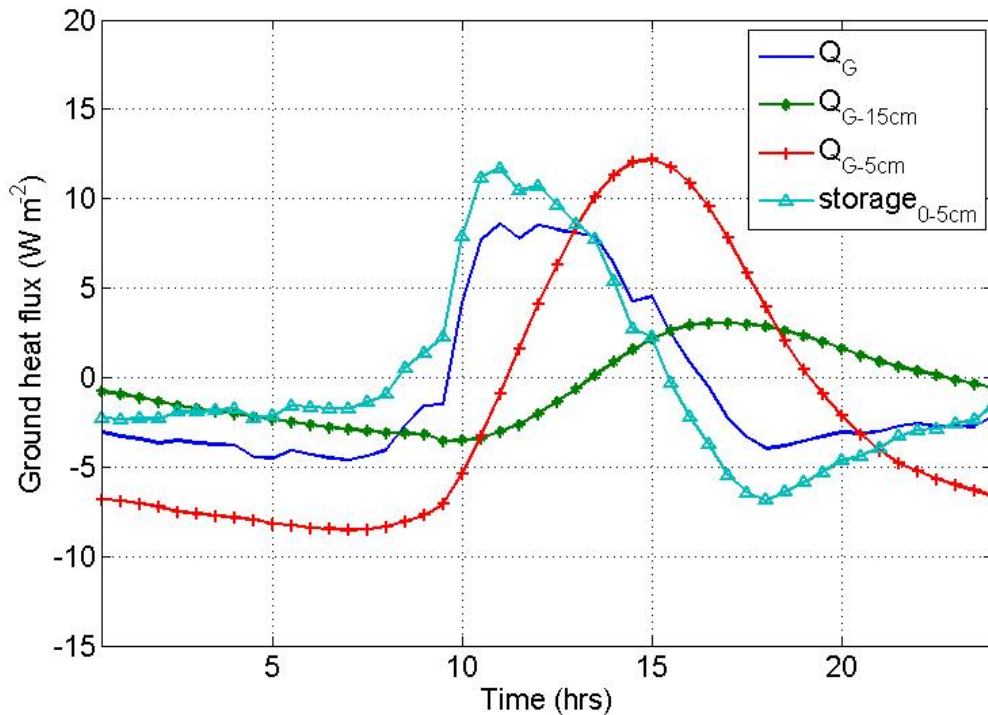


Figure 12. Partitioned diurnal ensemble ground heat flux terms for October – December 2014, where Q_G is the total ground heat flux, Q_{G-15cm} is the ground heat flux measured at -15 cm, Q_{G-5cm} is the ground heat flux at -5cm, and $storage_{0-5cm}$ is the change in heat storage between -1 and -5 cm. Measured on the living roof of the California Academy of sciences, San Francisco, Ca.

The storage heat flux term (0-5cm) registered an increase of heat flux at 08:00, and reached its peak around 11:00. Q_{G-5cm} registered a downward heat flux from 08:45, and more gradually increased until it peaked at 15:00. Q_{G-15cm} did not register heat conduction from the surface until 11:00, and peaked at 16:50. This indicates that there was a 2.25 hour lag time between the two heat flux plates registering conductive heat transfer, and a 1.5 hour lag time between the individual plates reaching their flux peak.

The storage heat flux began to decrease dramatically after 13:50, and decreased to -6.5 (W m^{-2}) by 18:00. $Q_{G-5\text{cm}}$ began decreasing more steeply at 16:00 and dropped continuously until -8 (W m^{-2}). $Q_{G-15\text{cm}}$ didn't start decreasing until 18:00, and then gradually declined throughout the night period with a minimum flux of -3.5 (W m^{-2}).

The magnitude of heat energy (W m^{-2}) also varied greatly between the two ground heat flux plates. $Q_{G-5\text{cm}}$ ranged between -10 and 17 (W m^{-2}), while $Q_{G-15\text{cm}}$ had a much narrower range of between -3.5 and 5.5 . This means that on an average diurnal basis, only 3 (W m^{-2}) of heat energy was conducted into the building below, and the remaining Q_G energy was stored in the substrate and later released in the evening.

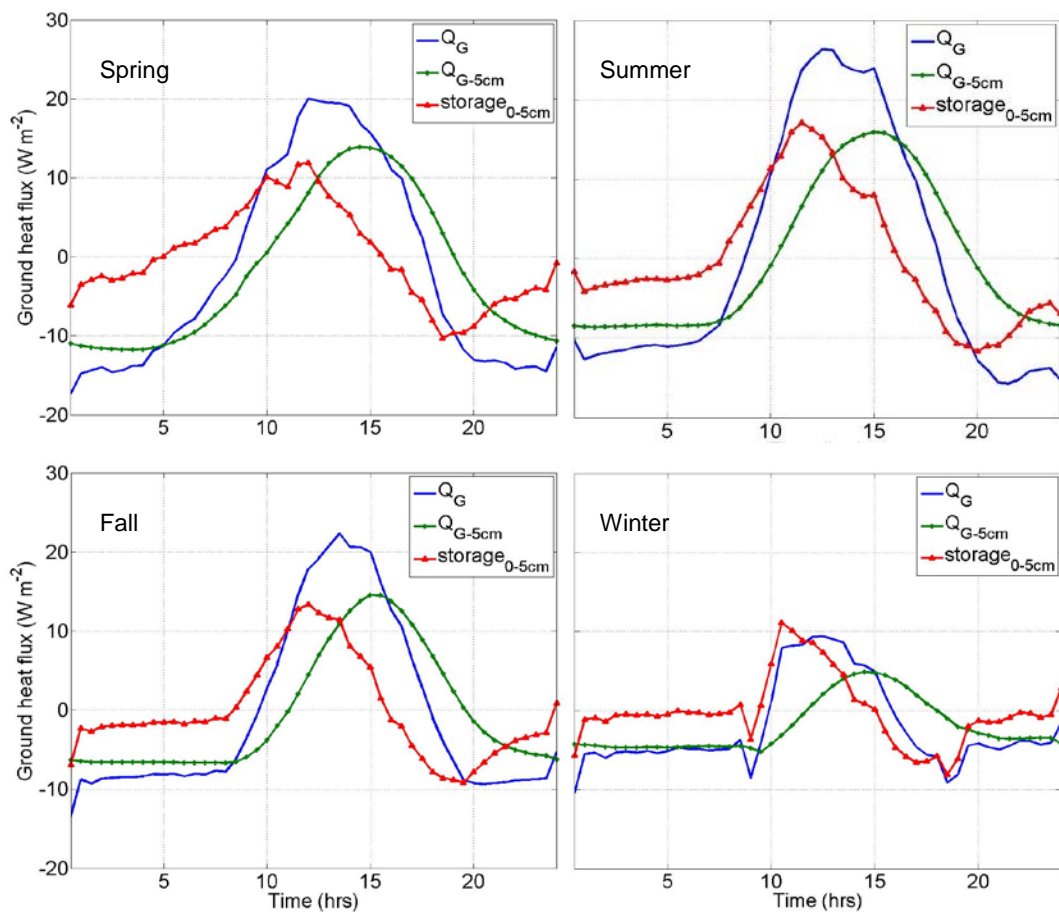


Figure 13. Seasonal variation in ground heat flux measurements on the living roof of the California Academy of Sciences, San Francisco, Ca, 2014.

The time lag is present for all seasons on the living roof. Although as Figure 13 shows, there is an even greater time lag between Q_G and Q_{G-5cm} in the winter. This is commensurate with the magnitude of the heat fluxes and indicates the smaller flux magnitudes correspond to a speed of conduction with depth.

Table 7. Monthly values of ground heat flux terms (in $MJ\ m^{-2}\ dy^{-1}$). Measured on the living roof of the California Academy of Sciences, San Francisco, Ca. October 2014 – February 2015.

	Q_{G-15cm}	Q_{G-5cm}	Q_G
	($MJ\ m^{-2}\ dy^{-1}$)		
10_Oct	-0.05	0.05	0.05
11_Nov	-0.18	-0.06	-0.07
12_Dec	-0.20	-0.14	-0.16
1_Jan	0.81	0.06	0.11
2_Feb	-0.15	-0.03	-0.02

4.5 Annual comparison

Because a preliminary study was conducted during the months of May June and July of 2013, inter-annual comparison between 2013 and 2014 of these summer months is possible. This is shown for the surface radiation budget (Figure 14) and for the surface energy balance (Figure 15).

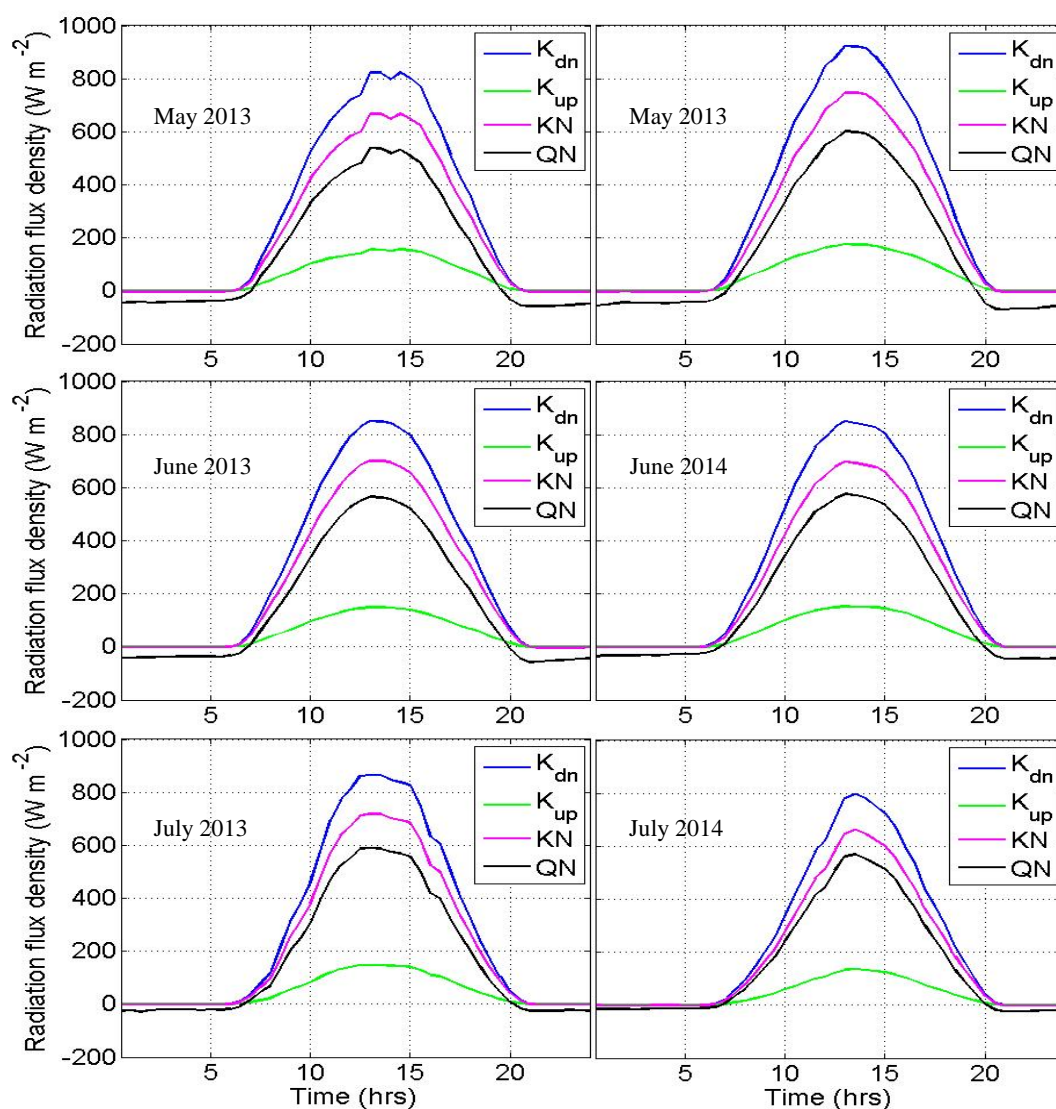


Figure 14. Daily ensemble averages of the surface shortwave radiation budget for the same three months in 2013 and 2014 on the living roof of the California Academy of Sciences in San Francisco Ca.

Table 8. Monthly total shortwave radiation for 2013 and 2014 ($n \text{ MJ m}^{-2} \text{ dy}^{-1}$) Measured on the living roof of the California Academy of sciences, San Francisco, Ca.

	Unit	May		June		July	
		2013	2014	2013	2014	2013	2014
(K_{dn})	MJ m^{-2}	23.95	26.08	24.90	24.97	24.03	20.23
(K_{up})	MJ m^{-2}	4.71	5.26	4.51	4.66	4.20	3.52

(KN)		19.24	20.82	20.39	20.31	19.83	16.71
(α)	(%)	19.6	20.1	18.1	18.6	17.4	17.3

Although there were slight variations between years, the overall surface radiation budget trends were relatively consistent in May and July, and nearly identical in June; this again reflects the climate profile for the time of year; with solar declination being the same, but also indicates that all three months, and June in particular had similar cloud cover as evidenced by their matching K_{dn} values. Using the same logic, it would appear that 2013 had slightly more cloud cover in May than 2014, and slightly less in July. Albedo in particular is relatively consistent between years (Table 8), indicating that the vegetation composition and coverage was similar.

Table 9. Monthly totals for 2013 and 2014 (in $\text{MJ m}^{-2} \text{ dy}^{-1}$) for the component parts of the surface energy balance. Measured on the living roof of the California Academy of Sciences, San Francisco, Ca.

	Unit	May		June		July	
		2013	2014	2013	2014	2013	2014
QN	$(\text{MJ m}^{-2} \text{ dy}^{-1})$	12.81	13.83	14.06	14.74	15.04	13.45
QE		5.37	4.74	5.00	3.54	4.57	3.82
QH		4.94	5.20	5.42	6.41	6.08	5.19
QG		0.01	-0.05	0.13	-0.01	0.11	-0.04
(β)		0.92	1.10	1.08	1.18	1.33	1.36
Residual		2.50	3.94	3.51	4.81	4.28	4.48

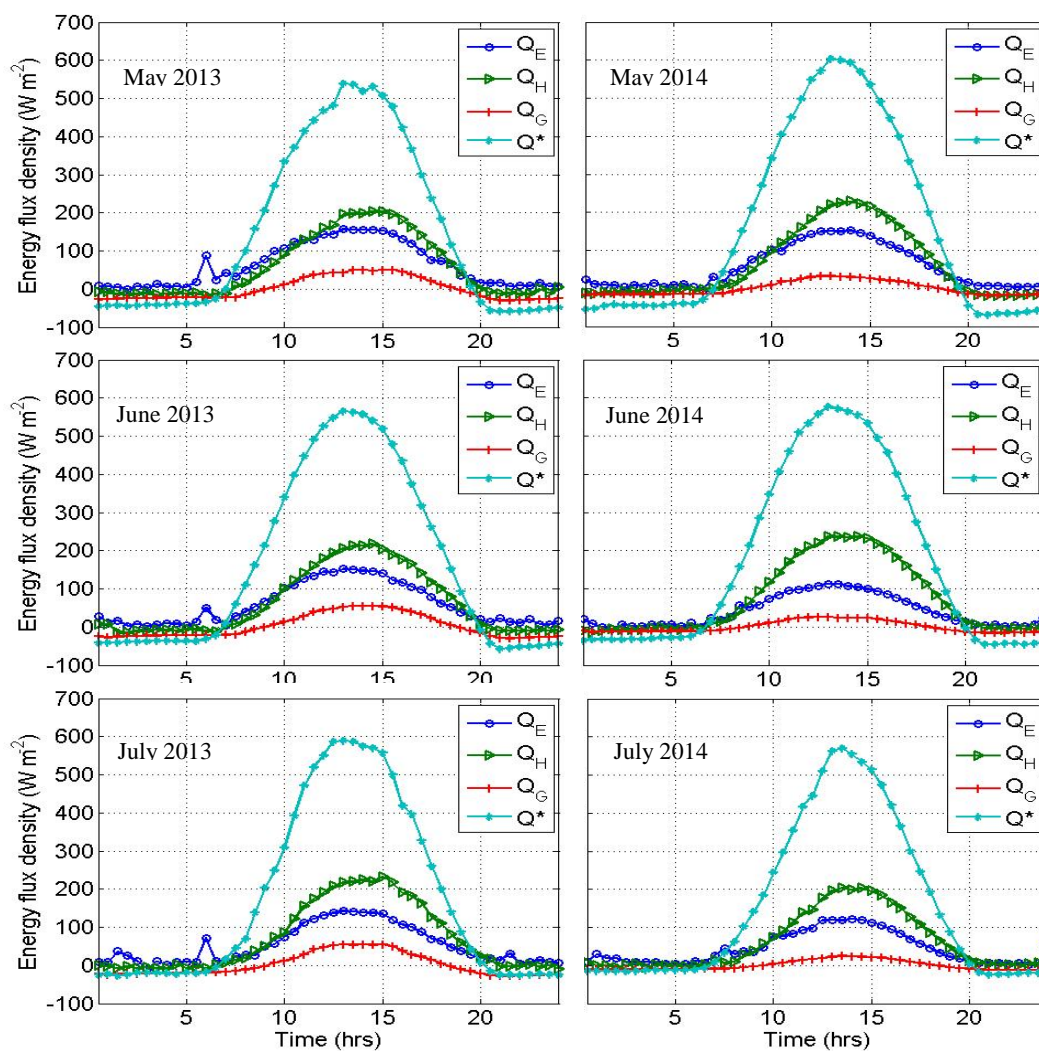


Figure 15. Daily ensemble averages of the surface energy balance for the same three months in 2013 and 2014 on the living roof of the California Academy of Sciences in San Francisco Ca.

While June of both years had nearly identical net radiation, the latent heat flux was noticeably larger in 2013 when it had a stronger presence over the sensible heat flux in the morning hours, and peaked roughly $50 \text{ (W m}^{-2}\text{)}$ higher than in 2014. The 2014 comparative deficit of Q_E was compensated for by an increase in Q_H . Q_G was also noticeably higher in 2013, which could be the result of increased volumetric water

content and thus increased soil heat capacity. Despite the similar patterns between years, Q_E was consistently greater in all three 2013 months, as was Q_G . Although in both 2014 and 2013 the sensible heat flux dominated the surface energy balance, leading to a Bowen ratio greater than 1 for both years.

4.6 Energy balance closure

The first law of thermodynamics theoretically requires the energy balance to close (Oliphant et al. 2004). Energy balance closure is achieved when all the terms on the right hand side of Equation 1 are equal to the term on the left (Q_N). Testing for energy balance closure often results in residual energy; that is, energy that is either being overestimated or underestimated in some way (Foken 2008, Wilson et al. 2002).

In order to isolate the turbulent fluxes from the remaining surface energy balance terms, the sum of Q_E and Q_H was plotted against Q_N minus Q_G for all available 30-minute periods (Figure 16). If the energy terms were balanced, each period would fall along a 1:1 line. The energy balance closure was assessed for the California Academy of Sciences' living roof resulting in turbulent heat fluxes that were 39% lower than available energy, though with very high consistency ($R^2=0.92$).

Potential reasons for this lack of closure include systematic bias in the instrumentation, energy sinks that were not considered (such as storage and advection), and the loss of both low and high frequency contributions to the turbulent fluxes (Wilson et al. 2002). In order to examine whether the latent or sensible heat fluxes were greater contributors to the underestimation of turbulent fluxes, observations were separated into high and low Bowen ratio values where high Bowen ratio was considered any value above 1.3, and low Bowen ratio was considered any value below 1.3 (Figure 17). This

showed that there was relatively little difference in closure under conditions dominated by the latent vs. sensible heat flux.

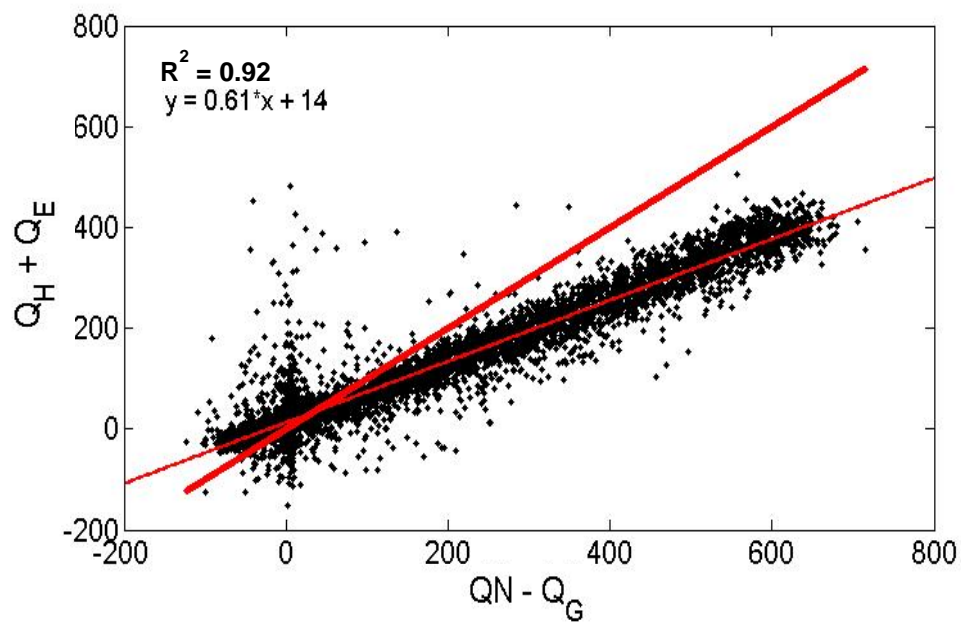


Figure 16. Energy balance closure (April 2014 – March 2015) on the living roof of the California Academy of Sciences in San Francisco, CA, where the thick red line is the 1:1 line and the thin red line is the linear regression trend

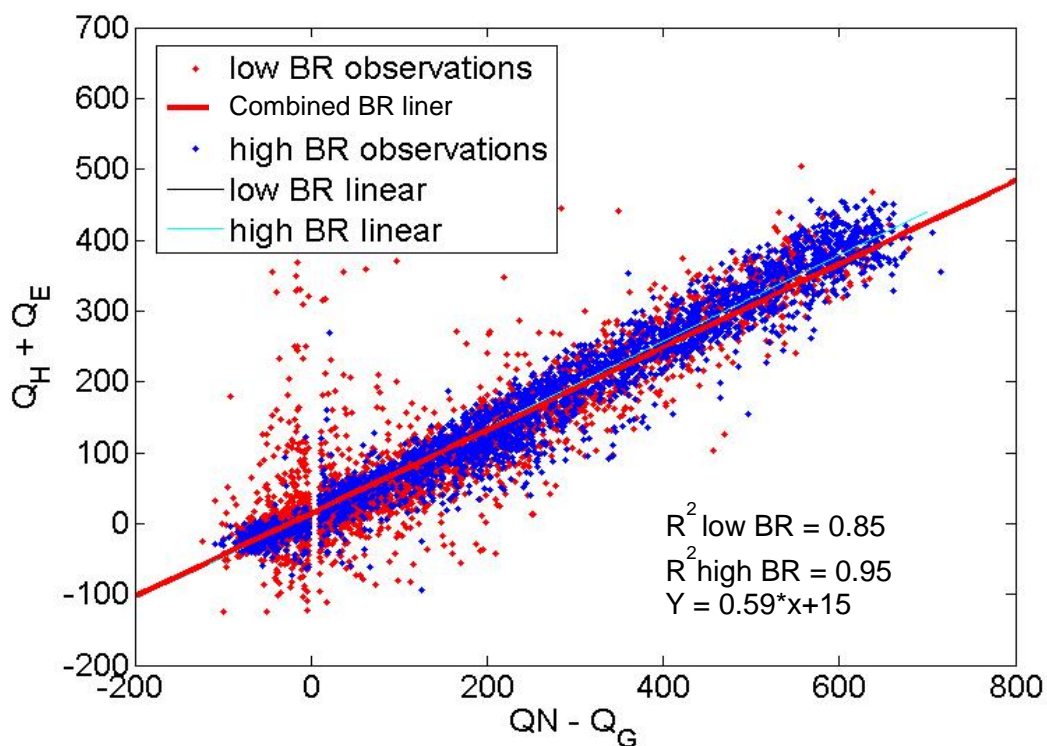


Figure 17. Energy balance closure (April 2014 – March 2015) on the living roof of the California Academy of Sciences in San Francisco, CA. Where low BR observations is Bowen < 1.3 and high BR observations is Bowen ratio > 1.3 .

5.0 Discussion

5.1 Surface albedo

One of the most commonly expressed benefits of living roofs is their ability to reflect heat energy (Sailor 2008). It has been argued that by reflecting rather than absorbing incoming solar radiation to a greater degree than standard roofs, living city surfaces mitigate the temperature gradient between urban and rural landscapes (Arnfield 2003, Pardo and Ferreira 2005). This theory however, depends on the nature of the non-living and living roofs, both of which vary significantly in color, leaf area index and vegetation height and density (Sailor 2008), producing a wide range in results. Takabayashi and

Moriyama (2007) found the albedo of a living roof (0.15) to be lower than a light gray concrete roof (0.37) while, Susca et al. (2011) found a living roof to have a greater albedo (0.20) than a comparative dark non-living roof, which was 0.05. Pardo and Ferreira (2005) found green colored roofs to be generally at the low end of the albedo spectrum (0.21) closest to ceramic roofs (0.20). The highest albedo belonged to white roofs (0.60), and the lowest to dark gray cement roofs (0.13). The annual albedo for the Cal Academy living roof was 0.20 making it a significant performing roof in terms of its ability to reflect incoming radiation when compared to standard roofs, and directly comparable to other living roof studies. The albedo of the Cal Academy roof exemplified how the surface vegetation mirrored the natural seasonal cycle of phenology and senescence. KN for the Cal Academy living roof was 13.18 ($\text{MJ m}^{-2} \text{ dy}^{-1}$). Using Oke's calculation for KN with a known albedo value, were the same amount of solar radiation to fall on a white roof ($\alpha = 0.60$), KN would be 6.60 ($\text{MJ m}^{-2} \text{ dy}^{-1}$), and for a black roof ($\alpha = 0.05$) KN would be 15.69 ($\text{MJ m}^{-2} \text{ dy}^{-1}$). Therefore on an annual basis the Cal Academy living roof absorbs double the incident radiation as a white roof, but 2.51 ($\text{MJ m}^{-2} \text{ dy}^{-1}$) less than a black roof.

Aside from Phenological changes in vegetation cover, albedo also changes over time (both daily and annually) depending on solar declination (Oke 1987). Because standard roofs have no vegetation, seasonal changes in albedo are due only to sun angle variations, assuming no slope: the lower the sun altitude, the greater the albedo, therefore on both living and standard roofs in North America, December and its adjoining months would have the lowest solar declination and the highest albedo observations, while June and its adjoining months would have the greatest declination and therefore

lowest albedo observations. However, on the Cal Academy living roof the highest albedo observations were made in April (0.22) at the height of the Mediterranean ecosystem growing season and the lowest in July (0.17) and August (0.18), when the vegetation turned dry and brown. The summer was also the season when the most weeding occurred to clear out dry dead weeds, leaving noticeable bare earth patches. In April the general plant color was a light bright green due to the thriving beach strawberry (32.9 % coverage) and the green California bent grass (11.8 % coverage). In the winter the beach strawberry changed to a red color while maintaining its same general % coverage. The colors green and red have been previously shown to have very similar albedo values (Pardo and Ferreira 2005). The observed surface area on the Cal Academy roof was horizontal, and did not take into account sun angle variations on the dome structures, and how the slope and aspect of these structures might impact the seasonal albedo of the roof.

5.2 Living roof controls on the surface energy balance

The cooling capacity of a living roof is due in part to an enhancement of the latent heat flux, and associated reduction in sensible heating of the overlying atmosphere (Rosenzweig et al. 2005, Berardi et al. 2014). This balance is well expressed by the non-dimensional Bowen ratio (β) which can be compared across urban and natural surfaces. β varies widely in urban areas depending on the climate and composition of the city (Grimmond and Oke 1995, Spronken-Smith et al. 1999) and has been found to correlate strongly and negatively with the fractional area of vegetation (Christen and Vogt 2004). Since this is generally low in urban areas, β tends to be high; around 5.0 (Oberndoffer et

al. (2007). By comparison to natural surfaces, this is equivalent to arid and semi-arid surfaces (e.g. Oliphant et al. 2011).

On the Cal Academy living roof, annual β was very close to unity (0.96). This is slightly higher than many natural ecosystems, which can range from 0.48 for wetlands, to 0.72 for coniferous forests (Eaton et al. 2001). However, studies conducted in similar Mediterranean climates have found β between 0.5 and 1.6 (Valentini et al. 1991); Other ecosystems with β close to 1.0 include South African mopane woodlands, Siberian pine forests (Oberndofer et al. 2007), and continental US grasslands (Kim and Verma 1989) where the similarity in β observations between studies could partially be explained by the 18.8% of grass land vegetation cover on the Cal Academy roof; the second largest plant-type present (Table 2), but is most likely explained by the general climactic similarities in precipitation and air temperature. The Cal Academy β was also comparable to a living roof in Hong Kong China, which had a β range between 0.72 for turf-grass cover and 0.90 for shrub cover (Jim and He 2010). This is surprisingly similar to the Cal Academy study when considering that Hong Kong is a subtropical humid climate with far more precipitation than San Francisco, and potentially indicates that the vegetation components and sub-surface drainage structure provided similar controls on latent and sensible heat; with Hong Kong having a similar surface layer construction and perennial peanut (*Arachis pinto*) as the predominant herbaceous vegetation cover, which is similar to beach strawberry in height, coverage and leaf area index. The Bowen ratio on the Cal Academy living roof fluctuated seasonally, with a standard deviation of 0.36. The highest Bowen ratios occurred in late summer (1.8 in July) with the lowest in winter and spring, corresponding both to the wet season and observed spring growth.

Although there were no adjacent standard roofs with which to compare observations, the Cal Academy roof, with a β just under 1, would likely produce a PCI effect if measured against a surrounding urban roof-surface. Perhaps the most comparable studied park space would be “mixed-use” due to the roofs observation deck, atrium and skylights. Such urban green spaces can have a PCI value of up to 3.8 ($^{\circ}\text{C}$) (Spronken-Smith et al. 1998). With their lack of water retention for evaporation, and plants for transpiration, it can be assumed that the entire magnitude of the latent heat would be added between the sensible and ground heat flux on a theoretical standard roof adjacent to the Cal Academy. As the annual Q_H and Q_G account for 38% and 11% of Q_N respectively, this would increase the sensible heat flux to 5.54 ($\text{MJ m}^{-2} \text{dy}^{-1}$), and ground heat flux to -0.77 ($\text{MJ m}^{-2} \text{dy}^{-1}$).

Although the Cal Academy applies light irrigation in summer, the seasonal plant functioning tends to follow a Mediterranean seasonal schedule with senescence in the second half of summer due to water stress and little activity in winter due to low light levels (Thorp et al. 2014). It is likely that this seasonal pattern in biome vegetation functioning, accounted for the lower Q_E observations (relative to Q_N) in late summer. The moderate increase in Q_E from July to August (0.04) cannot be accounted for by the nearly double increase in VWC, or there would be a likewise more significant jump in Q_E . A possible reason for this lack of relationship is that the Cal Academy living roof was too complex to tease out independent variables without controlling for other environmental factors that are present in the data. Atmospheric variables included available energy, air temperature, wind speed and vapor pressure deficit, while surface variables included the availability of water, plant species and soil porosity. With all of these variables acting at

different degrees on both temporal and geographic scales, no single variable other than QN stood out as a dominant control. Because the soil bulk density was low (0.81 g/cm^3), thus indicating a high volume of pore space, it is likely that water drained rapidly from the roof's surface, leaving less water available for VWC observations, and possibly contributing to the low correlation between Q_E and VWC. There was however an overall seasonal trend in increased Q_E and VWC signifying that while it was not the only or most dominant variable to control Q_E, there was a positively correlated relationship between the two.

5.3 Ground heat conduction and storage

Yet another touted benefit of living roofs is their ability to reduce the energy consumption of buildings by reducing heat conduction into and out of the building. Buildings account for roughly 40% of global energy use (Berardi et al. 2014). Ground heat flux was relatively stable and characteristic of other living roof studies (Tekebayashi et al. 2007, Feng et al. 2010). Daytime Q_G was typically around 10% of QN, which is similar to other vegetated surfaces (Wilson et al. 2002). Heat storage in the urban fabric (ΔQ_s) is very hard to measure accurately, and is often calculated as the residual in the energy balance. However, a review of urban studies show that heat storage accounts for up to 40% of the net radiation, a far larger portion than that of Q_G on the Cal Academy roof. These high observations of heat storage within urban structures also lead to high levels of evening heat emittance and increased UHI values (Oke 1989). Therefore Q_G on the living roof is yet another indicator of the roof's ability to mitigate the UHI effect.

Although no temperature sensors were installed within the Cal Academy's interior rooms, a 2007 study on living roof energy performance found a 6-49% reduction in

interior building temperature, and a 12-87% reduction in the room temperature directly below the roof (Santamouris et al. 2007). In natural ecosystems annual total Q_G values are typically near zero, and daily total Q_G values are typically small and slightly negative from summer to winter and positive from winter to summer, reflecting the seasonal change in soil temperature (Oliphant et al. 2004). The seasonally consistent negative values for daily Q_G indicate that the building below was, over the long term, conducting heat toward the substrate surface. This includes conduction through the concrete slab, waterproofing layer, synthetic insulation, impermeable drainage layer, and erosion control blanket. The Cal Academy roof is not an outlier in living roofs' heat conduction and storage capacity. The equivalent of Q_G for a study on a living roof in Guangzhou China had an identical ground heat flux that was likewise negative; indicating that that roof also emitted heat (Feng et al. 2010). The insulation properties of the substrate were displayed by the lag time and reduced magnitude between the heat flux observations at Q_{G-5} and Q_{G-15} which illustrate the living components of the roof act as natural insulation. This finding is consistent with a study conducted in the Mediterranean climate of Greece in 2003, where thicker substrate soil likewise exhibited a larger time lag and smaller variation of the thermal heat flux (Theodosiou 2003). This finding is also consistent with a 2010 living roof study in Hong Kong which likewise found substantial (2 hour) lag time in Q_G energy fluxes (Jim and He, 2010).

5.4 Controls on energy balance closure and sources of error

Controls on energy balance closure can include: Unstable vs. stable conditions, friction velocity, thermally induced turbulence, time of day, storage effects, and landscape heterogeneity (Franssen et al. 2010, Barr et al. 2006), horizontal and/or vertical

advection of heat, systematic errors associated with the sampling mismatch between the flux footprint and the sensors measuring other components of the energy balance, energy sinks that were not accounted for, and low and high frequency loss of turbulent fluxes (Wilson et al. 2002 B). While advection was systematically avoided by rejecting all periods when the 80th percentile of the cumulative flux distance fell outside of the roof area, advection on such a small complex and hilly terrain could lead to error. Although the instruments were installed with the objective of receiving the turbulent eddies from across the low-laying flat, eastern portion of the roof, it is possible that the domes topographically forced turbulence an advection in unaccounted for ways.

Energy balance closure resulted in an annual residual of 2.20 ($\text{MJ m}^{-2} \text{ dy}^{-1}$) and found that the turbulent heat fluxes underestimated the available energy by 39% based on linear regression. This underestimation was fairly consistent with an annual R^2 of 0.92. Lack of energy balance closure indicates that one or more parts of the surface energy balance equation were incorrectly measured. Either the turbulent heat fluxes were underestimated, the ground heat flux was underestimated, or the net radiation was overestimated. An increase of 2.20 ($\text{MJ m}^{-2} \text{ dy}^{-1}$) in the ground heat flux would be improbably large, therefore it is more likely that Q_N is overestimated, or that Q_H and Q_E are underestimated. Ground heat was likely measured with sufficient accuracy due to the measurements of soil bulk density (0.81 g/cm^3) calculated in spring of 2014. In order to determine which of the turbulent heat fluxes was being incorrectly measured, 30 min periods were divided into times of high and low Bowen ratio observations (Figure 17). The R^2 values of 0.85 and 0.95 for low and high observations respectively, indicate that underestimations of the turbulent heat fluxes were not significantly different when either

latent or sensible heat was dominant. This indicates if the eddy covariance technique is overestimating the turbulent heat fluxes, it is not producing greater errors under wet or dry conditions. Although the instruments were intentionally installed away from the leeward edge of the roof, turbulent flows resulting from roof-edge upwelling could have been measured.

6.0 For future study: Comparing latent heat flux

While the eddy covariance technique was successfully employed on the Cal Academy roof, it is not a useful study technique for replication because there are so few living roofs that offer the required footprint to achieve usable observations. In 2014, a preliminary weighing lysimeter device was installed adjacent to the eddy covariance tower to provide independent measurements of evapotranspiration. The function of the weighing lysimeter method is to measure the mass changes of soil and vegetation over 30 min periods. Over time, estimates of rainfall, irrigation and evapotranspiration are inferred. In order to determine mass changes, a volume of the desired substrate was excavated and placed into a container so that the volume of soil and vegetation was exposed to the atmosphere above, but completely confined within the impermeable container in all other directions. This became the “inner container”, and was then placed on top of a modified load cell within an outer container. The modified load cell was leveled on the bottom of the outer container using leveling screws. A small gap of approximately 5 mm was left between the walls of the inner and outer containers, thereby allowing the inner container housing the substrate to stand freely on the modified load cell, so that the entire force being measured by the load cell was representative of the inner container without interference from the surrounding substrate.

The weighing lysimeter method is independent from the eddy covariance technique, and thus provides a separate collection of data, from which the two independent values for evapotranspiration can be compared (Oliphant et al. in press).

$$F_{H_2O} = \frac{\Delta W_c}{A_c} \Delta t \quad (10)$$

where ΔW_c is the change in mass between averaging periods (g), A_c is the cross sectional area of the volume's surface and Δt is the time between averaging periods (0.5 hours). The weighing lysimeter was installed on the Cal Academy roof in September of 2014. Nesting containers were sawed down to the specific height of the Cal Academy's living roof substrate (15 cm), with the inner container sawed to a height of 10 cm to account for the thickness of the modified loadcell (5 cm). The result was a continuous surface of equal elevation between the lysimeter substrate and that of the surrounding living roof. The outer container measured 20 cm in diameter. The loadcell was wired into the data logger, and measurements were originally taken at 10 Hz, but then reduced to 5 S intervals to save space. A key component of the weighing lysimeter technique is to maintain the biophysical functioning of the substrate within the inner container. Without living flora, transpiration does not occur; only evaporation is measured. The vegetation within the inner container was monitored throughout the study and no adverse effects to plant growth and vitality were observed. This indicates that the field test-study has high potential for success, and future research could easily be compared with the energy balance results in this study.

7.0 Conclusions

This study provided over one year of data (2013-2015) on the component parts of the surface radiation budget and surface energy balance on the Cal Academy living roof.

Multiple climate variables such as precipitation and air temperature were measured, and both the plant and soil composition was assessed. An emphasis was placed on the partitioning of the surface energy balance between latent, sensible and ground heat fluxes, seasonality of all components, and controls on both radiative and heat flux observations. From the cumulative observations, the following conclusions can be drawn.

The 30-minute diurnal ensemble surface radiation budget components changed in magnitude over the seasonal time scale with a substantial decrease (range = 15.61 MJ m⁻² dy⁻¹) in incoming solar radiation between the summer and winter months due to the North American latitudinal location and corresponding sun angle. Longwave radiation changed little over the year compared to shortwave radiation. Net radiation was controlled by time of year and cloud cover, with diurnal ensembles observed under cloudy sky conditions resulting in as much as 125 (W m⁻²) less QN at peak times. The annual average albedo of 0.20 was directly comparable to other living roofs, higher than black (0.05) and dark grey (0.15) roofs, and lower only than light gray (0.37) and white (0.60) roofs, making it an overall significant performer at reflecting heat energy to offset UHI levels when analyzed on an annual scale. Albedo was seasonally controlled by phenological changes in plant color and coverage, which slightly superseded the control of solar declination which followed the anticipated seasonal trend for a northern latitude location.

The magnitude of the heat flux terms was strongly driven by available energy derived from the surface energy budget. This strong correlation led to a parallel decrease in magnitudes of heat fluxes from summer to winter. On an annual average,

latent heat surpassed sensible heat by $0.01 \text{ (MJ m}^{-2} \text{ dy}^{-1}\text{)}$ leading to a Bowen ratio of 0.96, indicating that the turbulent heat fluxes were relatively evenly partitioned. β was governed by seasonal changes in Q_N and to a lesser degree by phenology and the availability of water (VWC). β was highest in the late spring and early summer indicating that biophysical controls impacted Q_E and Q_H as evidenced by the switch from Q_H dominating the diurnal ensemble observations in the summer to Q_E dominating in the winter. Were no vegetation present on the Cal Academy roof, it can be assumed that the portion of Q_N occupied by this component would be partitioned into Q_H and Q_G , thus the cooling capacity of the living roof can be measured as the magnitude of Q_E , thereby demonstrating that the living roof offset the UHI by $3.19 \text{ (MJ m}^{-2} \text{ dy}^{-1}\text{)}$ on an annual average scale. The ground heat flux demonstrated the similarities between designed living roofs and natural substrate. Insulation of the building below was measured as the amount of heat energy that reached the surface vs. the amount of heat energy that reached the bottom of the 15 cm substrate; a small average diurnal maximum of $3 \text{ (W m}^{-2}\text{)}$ ever reach the building below. Seasonally Q_G remained negative every month, indicating that unlike a natural surface, a measurable amount of heat was conducted out of the building on an annual scale.

The sum of the turbulent heat fluxes ($Q_H + Q_E$) was found to underestimate the available energy ($Q_N - Q_G$) by 39%. However, no strong correlation was found between energy balance closure and times of Q_E or Q_H dominance, indicating that if they were incorrectly measured, the turbulent heat fluxes led to equal underestimation under times of either latent or sensible heat flux dominance. This study confirmed that living roofs do impact their local microclimates. UHI was offset primarily by the latent heat flux by an

average annual magnitude of $3.19 \text{ (MJ m}^{-2} \text{ dy}^{-1}\text{)}$, and by the ground heat flux, which accounted for around 10% of QN, significantly less than urban structures that can reach a maximum of 40% of QN. The living roof's albedo also offset UHI by reflecting the maximum (over 20%) amount of K_{dn} during the months with the highest vegetation % cover and when the plants were in their most vivacious bright green condition. The roof also impacted the climate of the interior building by only allowing a small annual average diurnal maximum of $3 \text{ (W m}^{-2}\text{)}$ to be conducted into the interior building.

8.0 References

Alessa, L. and Chapin, F.S. (2008) Anthropogenic biomes: a key contribution to earth-system science. *Trends in Ecology and Evolution*. 23, 529-531

Arnfield, A.J. (2003) Two decades of urban climate research: a review of turbulence, exchanges of energy and water, and the urban heat island. *International Journal of Climatology*. 23, 1-26

Baldocchi, D.D. (2003) Assessing the eddy covariance technique for evaluation carbon dioxide exchange rates of ecosystems: past, present and future. *Global Change Biology*. 9, 1-14

Baldocchi, D. D., Vogel, C. A. , Hall, B. (1997), Seasonal variation of energy and water vapor exchange rates above and below a boreal jack pine forest canopy, *Journal of Geophysical Research: Atmospheres*. 102, 28939–28951

Barbour, M.G, William, D. B. (1988) North American Terrestrial Vegetation, Cambridge University Press, Cambridge

Barr, A., Morgenstern, K., Black, T., McCaughey, J., Nesic, Z. (2006) Surface energy balance closure by the eddy-covariance method above three boreal forest

stands and implications for the measurement of the CO₂ flux. *Agricultural and Forest Meteorology*. 140, 322–337

Berardi, U., GhaffarianHoseini, A.H., GhaffarianHoseini, A. (2014) State-of-the-art analysis of the environmental benefits of green roofs. *Applied Energy*. 115, 411-428

Bladd, B.L., and Rosenberg, N.J. (1973) Lysimetric calibration of the Bowen ratio-energy balance method for evapotranspiration estimation in the Central Great Plains. *Journal of Applied Meteorology*. 13, 227-236

Bottyan, Z., Kircsi, A. Szegedi, S., Unger, J. (2005) The relationship between built-up areas and the spatial development of the mean maximum urban heat island in Debrecen, Hungary. *International journal of Climatology*. 25, 405-418

California Academy of Sciences (2014) Living Roof. Retrieved from:

<http://www.calacademy.org/exhibits/living-roof>

Castleton, H.F., Stovin, V., Beck, S.B.M., Davison, J.B. (2010) Green roofs; building energy savings and the potential for retrofit. *Energy and Buildings*. 42, 1582-1591

- Christen, A. and Vogt, R. (2004) Energy and radiation balance of a central European city. *International Journal of Climatology*. 24, 1395-1421
- Conomos, T.J., Smith, R.E., Gartner, J.W. (1985) Environmental Setting of San Francisco. *Hydrobiologia*. 129, 1-12
- Eaton, A.K., and Rouse, W.R. (2001) Surface energy balance of the western and central Canadian subarctic: variations in the energy balance among five major terrain types. *Journal of Climate*. 14, 3692-3703
- Eliasson, I. (2000) The use of climate knowledge in urban planning. *Landscape and Urban Planning*. 48, 31-44
- Feng, F., Meng Q., Zhang, Y. (2010) Theoretical and experimental analysis of the energy balance of extensive green roofs. *Energy and Buildings*. 42, 959-965
- Foken, T. (2008) The Energy Balance Closure Problem: An Overview. *Ecological Applications*. 18, 1351-1367
- Franssen, H.J., Stöckli, R., Lehner, I., Rotenberg, E., Seneviratne, S.I. (2010) Energy balance closure of eddy-covariance data: A multisite analysis for European FLUXNET stations. *Agricultural and Forest Meteorology*. 150, 1553–1567

- Grimmond, S. (2006) Applied climatology – urban climate. *Progress in Physical Geography*. 30, 270-279
- Grimmond, C.S.B., and Oke, T.R. (1995) Comparison Heat Fluxes from Summertime Observations in the Suburbs of North America. *American Meteorological Society*. 38, 922-940
- Hsieh, C., Katul, G., Chi, T. (2000) An approximate analytical model for footprint estimation of scalar fluxes in thermally stratified atmospheric flows. *Advances in Water Resources*. 23, 765-72.
- Hommer, B., Eliasson, I. (1999) Urban-rural vapor pressure deficit differences and their role in the development of urban heat islands. *International journal of Climatology*. 19, 989-1009
- Honjo, T., Narira, K., Sugawara, H., Mikami, T. (2003) Observation of Cool Island Effect in Urban parks (Shinjuku Gyoen). *Geographical Review of Japan*. 6, 403-420
- Howard, L. (1833) The climate of London deduced from meteorological observations Vol 1 Harvey and Darton, London
- Ichinose, T., Shimodozono, K., Hanaki, K. (1999) Impact of anthropogenic heat on urban climate in Tokyo. *Atmospheric Environment*. 33, 3897-3909

Jaffal, I., Ouldboukhite, S.E., Belarbi, R. (2012) A Comprehensive study of the impact of green roofs on building energy performance. *Renewable Energy*. 43, 157-164

Jansson C., Jansson, P.E., Gustafsson, D. (2007) Near surface climate in an urban vegetated park and its surroundings. *Theoretical and Applied Climatology*. 89, 185–193

Jim, C.Y., and He, H. (2010) Coupling heat flux dynamics with meteorological conditions in the green roof ecosystem. *Ecological Engineering*. 36, 1052-1063

Kalra, Y. P. (1996) Reference Methods for Plant Analysis, CRC Press, Taylor & Francis Group, LLC

Kim, J., and Verma, S.B. (1989) Components of surface energy balance in a temperate grassland ecosystem. *Boundary-Layer Meteorology*. 51, 417-1990

Liu, H., Randerson, J.T., Lindfors, J., Chapin, S. (2005) Changes in the surface energy budget after fire in boreal ecosystems of interior Alaska: An annual perspective. *Journal of Geographical Research*. 110, 1-12

- Martens, R., Bass, B., Alcazar, S. (2008) Roof–envelope ratio impact on green roof energy performance. *Urban Ecosystems*. 4, 399-408
- Masson, V., C.S.B. Grimmond, T.R. Oke (2002) Evaluation of the Town Energy Balance (TEB) Scheme with Direct Measurements from Dry Districts in Two Cities. *Journal of Applied Meteorology*. 41, 1011-1026
- Moncrieff, J.B., Massheder, J.M., de Burin, H., Elbers, J., Friborg, T., Heusinkveld, B., Kabat, P., Scott, S., Soegaard, H. Verhoef, A. (1997) A system to measure surface fluxes of momentum, sensible heat, water vapor and carbon dioxide. *Journal of Hydrology*. 188, 589-611
- Oberlander, G.T. (1956) Summer fog precipitation on the San Francisco Peninsula. *Ecology*. 37, 851-852
- Oke, T.R. (1987) *Boundary Layer Climates*, Routledge, London
- Oberndorfer, E., Lundholm, J., Bass, B., Coffman, R.R., Doshi, H., Dunnett, N., Gaffin, S., Kohler, M., Liu, K.K.Y., Rowe, B. (2007) Green roofs as urban ecosystems: ecological structures, functions, and services. *BioScience*. 57, 823-833

- Oke, T.R., Johnson, G.T., Steyn, D.G., Watson, I.D. (1991) Simulation of surface urban heat island under “ideal” conditions at night. Part 2; Diagnostics of causation. *Boundary layer Meteorology*. 56, 339-358
- Oke, T.R. (1980) The energetic basis of the urban heat island. *Quarterly journal of the Royal meteorology Society*. 108, 1-24
- Oke, T.R. (1973) City size and the urban heat island. *Atmospheric Environment*. 7, 769-779
- Oliphant, A.J., Grimmond, C.S.B., Zutter, H.N., Schmid, H.P., Su, H.B., Scott, S.L., Offerle, B., Randolph, J.C., Ehman, J. (2004) Heat storage and energy balance fluxes for a temperate deciduous forest. *Agricultural and Forest Meteorology*. 126,185-201
- Oliphant, A., Zawar-reza, P., Azizi, G., Dehghanpour, A., Harrison, J. (2011) Surface energy and water vapor fluxes observed in a desert plantation in central Iran. *Journal of Arid Environments*. 75, 926-935
- Oliphant, A.J. (2012) Terrestrial Ecosystem-Atmosphere Exchange of CO₂, Water and Energy from FLUXNET; Review and Meta-Analysis of a Global in-situ Observatory. *Geography Compass*. 10, 689-705

Pandey, S., Hinodliya, D.A., Mod, R. (2013) Experimental investigation on green roofs over buildings. *International Journal of Low-Carbon Technologies*. 8, 37-42

Pardo, R.T., and Ferreira, F.L. (2005) Measurement of albedo and analysis of its influence the surface temperature of building roof materials. *Energy and Buildings*. 37, 295-300

Rosenzweig, C., S. Gaffin, and L. Parshall (Eds.) (2006) Green Roofs in the New York Metropolitan Region: Research Report. Columbia University Center for Climate Systems Research and NASA Goddard Institute for Space Studies. New York. 59 pages.

Sailor, D.J. (2008) A green roof model for building energy simulation programs. *Energy and Buildings*. 40, 1466-1478

Saiz, S., Kennedy, C., Bass, B., Pressnail, K. (2006) Comparative life cycle assessment of standard and green roofs. *Environmental Science Technology*. 40, 4312-4316

Santamouris, M., Pavlou, C., Doukas, P., Mihalakakou, G., Synnefa, A., Hatzibiros, A., Patargias, P. (2007) Investigating and analyzing the energy and environmental performance of an experimental green roof system installed in a nursery school building in Athens, Greece. *Energy*. 32, 1781-1788

SF Department of Parks and Recreation (2014), Golden Gate Park Guide. Retrieved from <http://sfrecpark.org/>

Spronken-Smith, R.A., and Oke, T.R. (1998) The thermal regime of urban parks in two cities with different summer climates. *International Journal of Remote Sensing*. 11, 2085-2104

Spronken-Smith, R.A., Oke, T.R., Lowry, W. (2000) Advection and the surface energy balance across an irrigated urban park. *International Journal of Climatology*. 20, 1033-1047

Susca T., Gaffin, S.R., Dell'osso, G.R. (2011) positive effects of vegetation: urban heat island and green roofs. *Environmental Pollution*. 159, 2119-2126

Szegedi, S., Gyarmati, R. (2009) Impacts of urban green spaces on the spatial structure of the urban heat island in Debrecen and different sized settlements in its neighborhood. *ACTA Climatologicaet Chorologica*. 43,151-158

Tekebayashi, H. and Moriyama, M. (2007) Surface heat budget on green roof and high reflection roof for mitigation of urban heat island. *Building and Environment*. 42, 2971 2979

- Theodosiou, T.G. (2003) Summer period analysis of the performance of a planted roof as a passive cooling technique. *Energy and Buildings*. 35, 909-917
- Thorp, R. (2014) Observations of heat, water vapor and carbon dioxide exchanges over a living roof using eddy covariance. Thesis. San Francisco State University
- USGS (2012) Soil types and shaking hazard in the San Francisco Bay Area. Retrieved from: <http://earthquake.usgs.gov/regional/nca/soiltype/>
- Vallentini, R., De Angelis, P., Matteucci, G., Monaco, R., Dore, S., Scarscia Mugnozza, G.E. (1996) Seasonal net carbon dioxide exchange of a beech forest with the Atmosphere. *Global Change Biology*. 2, 199-207
- Weng, Q., Lu, D., Schubring, J. (2004) Estimation of land surface temperature – vegetation abundance relationship for urban heat island studies. *Remote Sensing of Environment*. 89, 467-483
- Wilson, K., Baldocchi, D., Aubinet, M., Berbigier, P., Bernhofer, C., Dolman, H., Falge, E., Field, C., Goldstein, A., Granier, A., Grelle, A., Halldor, T., Hollinger, D., Katul, G., Law, B., Lindroth, A., Meyers, T., Moncrieff, J., Monson, R., Oechel, W., Tenhunen, J., Valentini, R., Verma, S., Vesala, T., Wofsy, S. (2002) Energy partitioning between latent and sensible heat flux during the warm season at FLUXNET sites. *Water Resources Research*. 38, 1294-1318

Williams, N.S.G, Rayner, J. P., Raynor, K. (2010) Green roofs for a wide brown land: opportunities and barriers for rooftop greening in Australia. *Urban Forestry & Urban Greening*. 9, 245-251.

Wofsy, S.C., Goulden, M.L., Munger, J.W., Fan, S.M., Bakwin, P.S., Daube, B.C., Bassow, F. A., Bazzaz, S.L. (1993) Net exchange of CO₂ in a mid-latitude forest. *Science*. 260, 1314-1317

Xu, L. Baldocchi, D.D. (2004) Seasonal variation in carbon dioxide exchange over a Mediterranean annual grassland in California. *Agriculture and Forest meteorology*. 1232, 79-96